

## MIT Open Access Articles

### *Radar Diagnosis of the Thundercloud Electron Accelerator*

The MIT Faculty has made this article openly available. **Please share** how this access benefits you. Your story matters.

**Citation:** Williams, E., Mkrtchyan, H., Mailyan, B., Karapetyan, G. and Hovakimyan, S. 2022. "Radar Diagnosis of the Thundercloud Electron Accelerator." 127 (11).

**As Published:** 10.1029/2021jd035957

**Publisher:** American Geophysical Union (AGU)

**Persistent URL:** <https://hdl.handle.net/1721.1/144144>

**Version:** Final published version: final published article, as it appeared in a journal, conference proceedings, or other formally published context

**Terms of use:** Creative Commons Attribution-NonCommercial-NoDerivs License








## RESEARCH ARTICLE

10.1029/2021JD035957

# Radar Diagnosis of the Thundercloud Electron Accelerator

E. Williams<sup>1</sup> , H. Mkrtchyan<sup>1,2</sup> , B. Mailyan<sup>2,3</sup>, G. Karapetyan<sup>2</sup> , and S. Hovakimyan<sup>4</sup> 

### Key Points:

- Thunderstorm Ground Enhancements (TGEs) are indicative of downward electron acceleration within the storm and are manifest with both polarities of the electric field
- Vertical development disclosed by RADAR is uniquely linked with "positive" and "negative" TGEs
- These different vertical developments are attributed to a temperature-dependent tripole structure of thunderclouds

### Correspondence to:

E. Williams,  
earlerw@mit.edu

### Citation:

Williams, E., Mkrtchyan, H., Mailyan, B., Karapetyan, G., & Hovakimyan, S. (2022). Radar diagnosis of the thundercloud electron accelerator. *Journal of Geophysical Research: Atmospheres*, 127, e2021JD035957. <https://doi.org/10.1029/2021JD035957>

Received 29 SEP 2021  
Accepted 15 MAR 2022

### Author Contributions:

**Conceptualization:** E. Williams  
**Data curation:** H. Mkrtchyan  
**Formal analysis:** E. Williams, H. Mkrtchyan  
**Investigation:** E. Williams, H. Mkrtchyan, B. Mailyan, G. Karapetyan  
**Methodology:** E. Williams, H. Mkrtchyan, B. Mailyan  
**Project Administration:** E. Williams  
**Resources:** E. Williams, H. Mkrtchyan, B. Mailyan, G. Karapetyan, S. Hovakimyan  
**Software:** H. Mkrtchyan, B. Mailyan, G. Karapetyan, S. Hovakimyan  
**Supervision:** E. Williams  
**Validation:** H. Mkrtchyan  
**Visualization:** H. Mkrtchyan, G. Karapetyan, S. Hovakimyan

© 2022. The Authors.

This is an open access article under the terms of the [Creative Commons Attribution-NonCommercial-NoDerivs License](https://creativecommons.org/licenses/by-nc-nd/4.0/), which permits use and distribution in any medium, provided the original work is properly cited, the use is non-commercial and no modifications or adaptations are made.

<sup>1</sup>Massachusetts Institute of Technology, Cambridge, MA, USA, <sup>2</sup>A. Alikhanian National Science Lab, Yerevan, Armenia, <sup>3</sup>Center for Astro, Particle and Planetary Physics, New York University, Abu Dhabi, United Arab Emirates, <sup>4</sup>Antihail Service, Hydrometeorology and Monitoring Center, Yerevan, Armenia

**Abstract** Thunderstorm Ground Enhancements (TGEs) refer to correlated enhancements in surface electric field and gamma ray flux that are manifestations of electron runaway in the storm overhead. The electric field enhancements can be of positive or negative polarity. In this study, altitude-resolved S-band radar observations of graupel are used to demonstrate distinct differences in storm structure linked with these “positive” and “negative” TGEs. The physical interpretation rests on the well-established temperature-dependent tripole structure of thunderstorms, with the main negative charge of the tripole acting as an electron repeller. This interpretation is supported by case studies showing altitude-stable convection, with shallow (deep) development linked with “positive” (“negative”) TGEs, and by case studies of collapsing storms that show upper dipole dominance early and lower inverted dipole dominance later when graupel particles descend from a colder to warmer temperature domain. In the case of many TGEs on Mt Aragats (3.2 km MSL), the temperature-dependent altitude of downward electron acceleration and avalanching may be sufficiently distant (>500 m) from surface detectors that the energetic electrons (1–10 MeV) are not likely avalanche/runaway electrons. Instead, they are Compton-scattered and pair-produced electrons from bremsstrahlung gamma radiation emanating from the high-field avalanche region aloft. These inferences are consistent with GEANT4 calculations that identify the physical origins of energetic electrons at the surface.

## 1. Introduction

C.T.R. Wilson (1925) predicted that electrons would run away to GeV energies in the quasi-DC electric field of a thunderstorm. This prediction for kilometer-scale behavior was evoked by laboratory observations at centimeter scales in Wilson's cloud chamber that showed tracks of individual electrons straightening with increasing energy (Wilson, 1923), and by J.J. Thomson's theory that the collisional cross section diminished monotonically with increasing electron energy. Though Wilson was aware of remarkable but infrequent collisions of electrons with the nuclei of atoms in his cloud chamber (Wilson, 1923), he chose to de-emphasize this key source for bremsstrahlung (breaking radiation) in his landmark 1925 paper (Wilson (1956) later corrected this omission of bremsstrahlung.).

Thunderstorm Ground Enhancements (TGEs) are today the recognized manifestation of Wilson's runaway electrons beneath thunderstorms. They have been shown to occur in the presence of exceptional magnitudes of the electric field. From the earliest searches for runaway electrons (Schonland, 1930; Wilson, 1929) to today (Chilingarian, Hovsepian, Svechnikova, & Zazyan, 2021), the main negative charge of the thunderstorm has served as the repulsive accelerator of electrons, downward below it and upward above it (Wilson, 1929; see also Figure 1). Ironically, the key “enhancement” in TGEs at the ground (in addition to the magnitude of the electric field) is the downward gamma radiation Wilson had de-emphasized and produced by the bremsstrahlung from the accelerated electrons in the avalanche region beneath the main negative charge (Chilingarian, Hovsepian, Svechnikova, & Zazyan, 2021). The range of gamma rays in the air is an order of magnitude larger than that of electrons of the same energy (Evans, 1955), and so the gamma rays can serve as a messenger for electron acceleration for the breakdown field higher in the storm.

TGEs have now been documented at elevated observatories worldwide in summer, and at sea level in winter when the strong field region is substantially closer to the surface observations (e.g., Torii et al., 2011; Wada et al., 2021). The richest archive of TGEs is found at Mt Aragats in Armenia, the site of the present investigation. More than 500 cases have been documented there (Chilingarian, Hovsepian, Svechnikova, & Zazyan, 2021). Clear evidence for TGEs in both strong positive and negative fields is now prevalent. In the early years of research on TGEs, the negative E field polarity appeared systematic (Chilingarian, 2014; Chilingarian et al., 2011, 2012).

Writing – original draft: E. Williams,  
H. Mkrtychyan  
Writing – review & editing: E.  
Williams, H. Mkrtychyan, B. Mailyan

But as more cases were documented and examined, TGE occurrences with both E field polarities were demonstrated (Chilingarian, Hovsepian, et al., 2018). The working hypothesis for these bipolar TGEs in general observations is the acknowledged presence of two spatially separated dipole polarities in thunderstorms (Figure 1). This hypothesis is not a new one (Chilingarian & Mkrtychyan, 2012). What is new in the present study is the integration of observational assets at Mt Aragats, most notably radar observations, to show physical distinctions in storm structure linked with “positive” and “negative” TGEs.

Electric dipole maintenance in thunderstorms is widely recognized to originate from collisions between large and small ice hydrometeors, with selective charge transfer in the collision, followed by the kilometer-scale dipole creation by gravitational forces. Radar is especially well-suited for remote sensing of the large ice particles (most commonly graupel) in any cloud-scale dipole because the theoretical radar cross section of hydrometeors varies as the sixth power of the particle diameter (e.g., Battan, 1973).

The superposition of two distinct dipoles is the widely-recognized tripole structure (Figure 1) of thunderstorms (Williams, 1989). Based on extensive electric field soundings of storms in England (Simpson & Robinson, 1940; Simpson & Scrase, 1937), the tripole was offered up by G.C. Simpson as a compromise with C.T.R. Wilson in their long-standing debate pertaining to the dipole polarity of thunderstorms (Austin, 2001; Williams, 2009). Kuettner (1950) later made observations of the surface electric field and air temperature on the Zugspitze in Germany, at an altitude similar to Mt. Aragats and gave temperature assignments to the charge centers of the Simpson tripole. Kuettner (1950) also gave the names “graupel dipole” and “snow dipole” to the electrical features now linked with bipolar TGEs. (Subsequent terminology used in this paper will identify “main positive dipole” with the “snow dipole” and “inverted dipole” with the “graupel dipole”). The consistent temperature

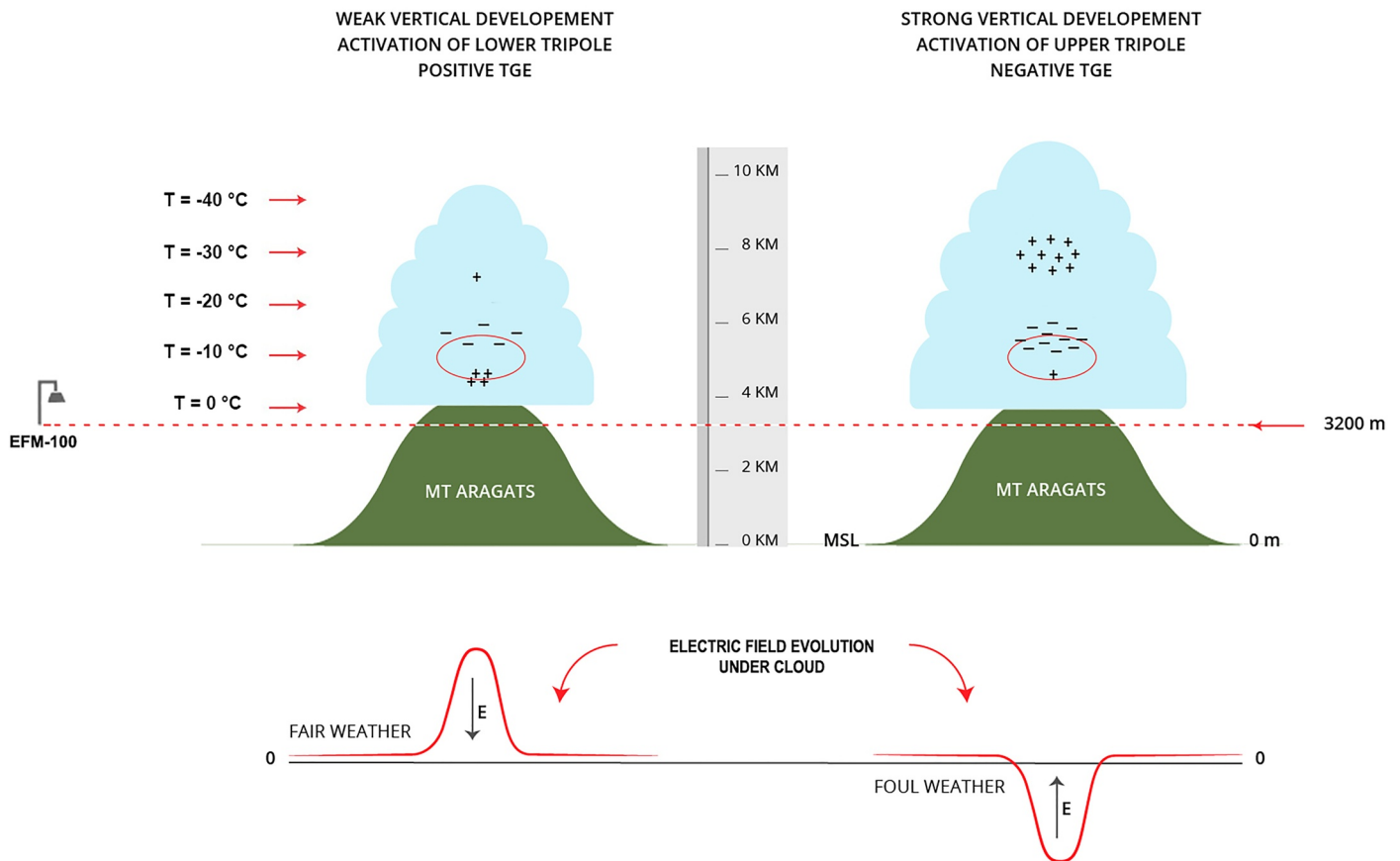


**Figure 1.** Cartoon illustrating full tripole structure for deep (and colder) convection with “negative” Thunderstorm Ground Enhancements (TGE) (right side), and bottom heavy tripole for shallow (and warmer) convection with “positive” TGE (left side). The region of downward electron acceleration (red oval) in these two scenarios lies beneath the main negative charge region in both the “positive TGE” (left) and the “negative TGE” (right). Most typically in summer conditions the Aragats peak (4090 m MSL) is above cloud base but the Aragats station is below cloud base, as shown.

dependence of thunderstorm electrical structure was later solidified by lightning charge analysis (Jacobson & Krider, 1976; Krehbiel et al., 1983; Krehbiel, 1981, 1986) that had been originated by Wilson (1916). The lower positive charge center (LPCC) was de-emphasized in much of the lightning charge analysis, but the analysis did not belie its existence (e.g., Maier & Krider, 1986). The extensive evidence for the tripole structure of thunderclouds then available was reviewed three decades ago (Williams, 1989). However, noteworthy new evidence has emerged more recently based on remote sensing methods of radar and radio-frequency lightning detection. The polarity asymmetry of VHF emission from lightning leaders (e.g., Williams, 2006) has been especially important in allowing remote sensing of storm electrical polarity (Li et al., 2020; Zheng et al., 2018).

On the basis of dual pole radar and LMA observations, Bruning et al. (2007) found evidence for a dominant inverted dipole in a situation with limited radar development into the cold part of the atmosphere. In later related modeling work, Mansell et al. (2010) referred to the Bruning storm as a “bottom heavy tripole” and also recognized a full range of tripole invariants (Figure 12). Takahashi (2012) documented temperature-dependent tripole structure with in situ measurements in rainbands in Micronesia.

In studies of thunderstorms on the Tibetan Plateau with a VHF lightning location network and a C-band Doppler radar, Li et al. (2020) showed evidence for inverted dipole structure in early shallow stages of storm development (to a temperature of  $-17^{\circ}\text{C}$ ) and full tripole structure as the storm developed further to  $-40^{\circ}\text{C}$  and colder.

In studies of winter thunderstorms at sea level in Japan with a 9-station LMA network and a JMA weather radar, Zheng et al. (2018) found inverted storm polarity when the radar echo was confined to temperatures “warmer” than  $-10^{\circ}\text{C}$ . In contrast, the deepest, coldest convection (to temperatures  $< -30^{\circ}\text{C}$ ) most commonly showed a full tripole structure. Takahashi et al. (1999, 2019) have also documented temperature-dependent tripole structure in winter storms in Japan by in situ measurements.

The discovery of inverted dipole formation (in advance of the main positive dipole) in the early shallow development of isolated summer thunderstorms (Stolzenburg et al., 2015; Karunarathna et al., 2017; Cummins et al., personal communication, 2021) and the predominance of downward-directed electric field over shallow convection in off-season storms (Anderson, 1966; Markson & Anderson, 1988; when the key isotherms are lower in MSL altitude) can both be taken as additional evidence for a temperature-dependent tripole structure.

In the present study, 4D (x,y,z,t) S-band radar observations will be used with nearby temperature soundings to identify distinct differences in vertical storm structure linked with “positive” and “negative” TGEs over Mt Aragats. Electric field measurements beneath a thunderstorm are normally non-uniquely related to the distribution of charge overhead. The vertical resolution afforded by the radar observations overcomes this problem of nonuniqueness.

## 2. Methodology

### 2.1. Aragats Station

Mt Aragats is the site for this study on the mountain storms that are accelerators of electrons. The mountain itself is a large dormant stratovolcano (Karakhainian et al., 2003) in North-West Armenia about 50 km from Armenia's capital Yerevan. It is the highest peak in modern Armenia and in the Lesser Caucasus range. Aragats is a circular, shield-like mountain composed of four summits, Northern (the highest, 4,090m), Western (4,080m), Southern (3,879 m), and Eastern (3,916 m) forming the rim of a volcanic crater. The Aragats research station of the Cosmic Ray Division (CRD) of the Yerevan Physics Institute (YerPhI) is located near Lake Kari at 3,200 m altitude (latitude:  $40^{\circ}28'N$ ; longitude:  $44^{\circ}10'E$ ). At the Aragats station, the average winter temperature is  $-15^{\circ}\text{C}$ , with minimum values reaching down to  $-40^{\circ}\text{C}$ . The average summer temperature is  $12^{\circ}\text{C}$  with the maximum reaching  $20^{\circ}\text{C}$ . Average surface wind speed in summer is 6 m/s and in the winter, it is 10 m/s occasionally reaching 40 m/s. During thunderstorms sometimes the cloud base is reaching Aragats station and commonly it varies between 50 m and 1 km.

The Aragats cosmic ray research station operates year-round. Detectors for observations of high-energy atmospheric phenomena and routine weather station data are logged continuously and also forwarded to the main campus of the Yerevan Physics Institute for archival. Online visualization programs ADAS (Chilingarian et al., 2011) and ADEI (Chilingaryan et al., 2010) provide online access to more than 300 time series.

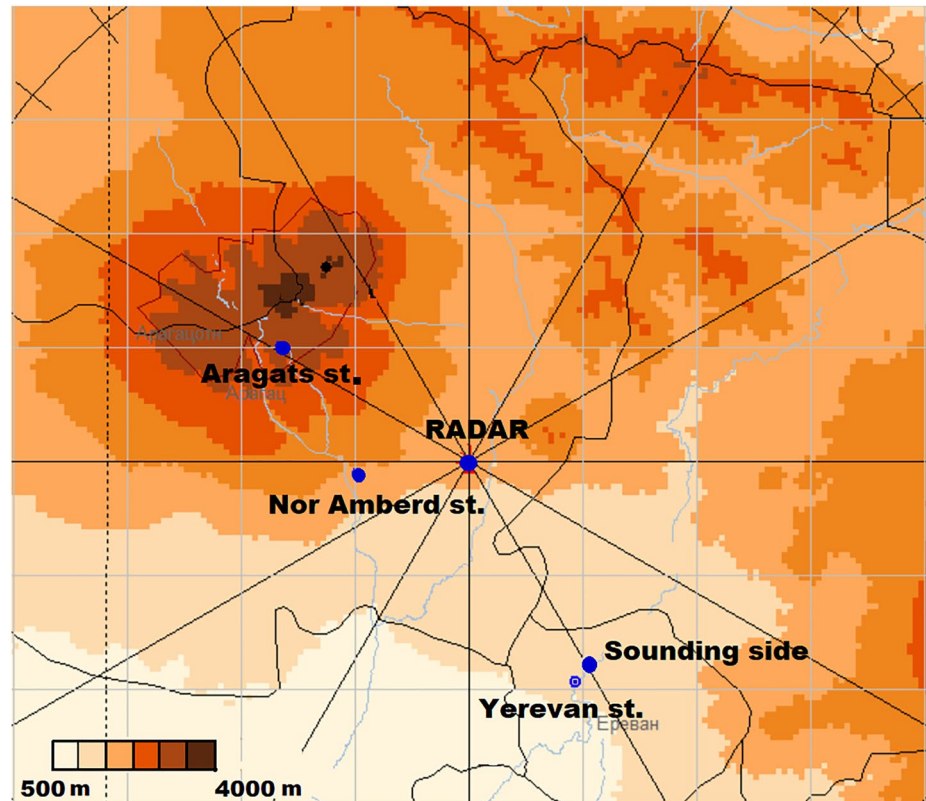


**Figure 2.** Locations of the S-band radar and measurement stations (Aragats, Nor Amberd, Yerevan, and sounding site). Radar distance from the Aragats station is 19 km. Elevation of the terrain is color-coded.

## 2.2. Nor-Amberd Research Station

The Nor-Amberd Research Station (40.37 N, 44.26 E, 2,000 m MSL) is located on the slopes of Mt. Aragats, approximately 26.5 km northwest of Yerevan and near the famous twelfth century Amberd fortress. It is 12.8 km distant from the Aragats Research Station (Figure 2). This station is equipped with a similar suite of measurements to the main station.

## 2.3. Surface Electric Field Measurements

The monitoring of the bipolar surface electric field is of fundamental importance in this study. All stations of the Cosmic Ray Division (see Figure 2 for all station locations) are equipped with electric field mills of the type Boltek EFM-100 (for details, see <http://www.boltek.com/>). Four separate Boltek instruments are installed at the Aragats Space Environmental Center (ASEC). Another two sensors are located at the Nor Amberd station and at the Yerevan station. The same Boltek electric field instrument at the Aragats station is used for all eight case studies reported here.

All electric field time series are sampled continuously at a rate of 20 Hz. In addition to recording electric field, this Boltek EFM also estimates the distance to flash locations based on analysis of abrupt electric field changes. The accuracy of the electric field measurement is of the order of 20%–30%. The same sign convention for electric field is used throughout this study: a dominant positive (negative) charge overhead causes a positive (negative) field.

## 2.4. Particle Detectors

For this study, we have used several particle detectors to show the accuracy of enhancements of the particle fluxes in TGEs. The detectors used are STAND1, SEVAN, and ASNT, described in more detail below. The network

**Table 1**  
*Summary of Radiation Detector Characteristics Calculated Based on 14 June 2020 Observations*

Detector type	Surface area in (m <sup>2</sup> )	Mean count rate during 2 hours	Detection thresh. (MeV)	Stand. deviation (SD)	No of SD	γ detect. efficiency [%] at 10 MeV	Reference
ASNT	1	2127	4	46	11.8	1	Chilingarian, Hovsepyan, and Zazyan (2021)
NaI #5	0.032	2709	3	53	15.6	80	Avakyan K. et al. (2013)
STAND 1 cm	1	45,868	0.8	570	73	98	Chilingarian, Karapetyan et al. (2013)
STAND 3 cm (1 s)	1	435	3	21	4.3	4.4	Chilingarian, Vanyan, et al. (2013)
SEVAN upper	1	28,781	7	174	28.7	1	Chilingarian et al. (2018b)

of detectors located at the Aragats research station has registered electrons, muons, gamma rays, and neutrons since 1943 (Chilingarian et al., 2005). The detectors are operated 24 hr, 7 days, and 12 months. The frequency of the data stream from particle detectors now reaches hundreds of kHz (Chilingarian et al., 2019). The registered time series are saved in local servers and are accessible to users worldwide. The data are free for general use in a special WEB data analysis platform, which is the advanced multidimensional visualization system ADEI (Advanced Data Extraction Infrastructure). With the help of ADEI it is possible to handle large amounts of stored data (Chilingarian et al., 2019).

The “Stand 1 cm” detector consists of a three-layer assembly of 1 cm thick 1 m<sup>2</sup> sensitive plastic scintillators, which are placed one above the other. This detector is located outside the building at the Aragats research station. For this study, we have used the upper plastic scintillator of the STAND 1 cm. The energy threshold is ~0.8 MeV (Chilingarian et al., 2019). The detection of charged flux by scintillators has very high efficiency (98%–99%), though the efficiency of detecting neutral flux is highly suppressed and is of order 1%–2% (Chilingarian et al., 2012).

Data from the Stand 1 cm detector have been compared with the SEVAN detector. The Space Environmental Viewing and Analysis Network (SEVAN) is a system of particle detectors located at middle and low latitudes which register primary cosmic rays with an energy of more than 7 GeV. It is assembled from scintillators with 3 assembled layers. The energy threshold of the upper scintillator of the SEVAN detector is 7 MeV. The combination of the layers allows for the registration of different particle types.

For some particle measurements, the Aragats Solar Neutron Telescope (ASNT) was also used (described in Chilingarian, Hovsepyan, Svechnikova, & Zazyan, 2021) as a detector. It is installed inside the MAKET building. The ASNT is formed from 4 separate identical modules (see Chilingarian, Hovsepyan, Svechnikova, & Zazyan, 2021). Each module consists of standard slabs of 50 × 50 × 5cm<sup>3</sup> plastic scintillators stacked vertically on a 100 × 100 × 10 cm<sup>3</sup> horizontal plastic scintillator slab. The total thickness of the assembly is 60 cm. Four detectors of 100 × 100 × 5cm<sup>3</sup> size each are located above the thick scintillator assembly and are used to indicate vertical traversal of the charged particles. Energy releases in the top or bottom scintillators are conditioned on the absence of signal in correspondingly lower and upper layers and on minimal energy release. The energy threshold in the upper monitors is 4 MeV (see Chilingarian, Hovsepyan, Svechnikova, & Zazyan, 2021).

The NaI crystal is a scintillator in a sealed aluminum (1-mm-thick) housing located beneath the roof of the SKL building. The NaI energy threshold is 0.3 MeV. The efficiency for gamma ray detection is ~80%. Detector details are presented in Table 1.

## 2.5. Radar Methodology

This study was enabled by the discovery of a fully-operational S-band radar at short range (19 km) from the rich suite of nuclear physics and electrical measurements at Mt Aragats. This radar facility, shown in Figure 3 with Mt Aragats rising in the background to the northwest, is a Soviet-era MRL-5 brand. This dual wavelength (S-band and X-band) radar, designed specifically for hail detection, is currently deployed not only in Armenia, but in ~45 other countries including Cuba (Koloskov et al., 1996; Pena et al., 2000), Poland (Moskowicz et al., 1994), Russia (AbshaeV et al., 2019, 2020), and South Africa (Visser, 2001). The characteristics of the MRL-5 radar are summarized in Table 2.



**Figure 3.** S-band radar site with Mt. Aragats in the background.

The rapid scan rate for this radar, with the completion of full 360-deg PPI scans at 18 separate elevation angles in only 200 s is well suited to the interests of this study, given typical durations of TGEs of order 5 min (see Table 2). The attendant short radar dwell times reduce the accuracy of the reflectivity estimates somewhat (e.g., Battan, 1973), but absolute reflectivities are fortunately not crucial for this study.

A special software package (Abshaev et al., 2019, 2020) is used to convert the PPI-based volume scans to 3D cartesian CAPPI (Constant Altitude Plan Position Indicator) data, with 500-m resolution. Reflectivity estimates on these 3D grids were available with a resolution of 1, 2, and 5 dBZ, of which we preferred 2 dBZ resolution for purposes of color display.

**Table 2**  
*S-Band (MRL-5) Radar Parameters*

Characteristics	Units
Altitude of radar site	1634 m MSL
Wavelength	10 cm
Antenna diameter	4.5 m
Beamwidth	1.3 deg
Azimuthal resolution over Aragats (19 km range)	420 m
Pulse length	2 microseconds (300 m)
Pulse repetition frequency	250 Hz (7–9 pulse per 3 deg azimuth)
Volume scan description	18 elevation angles between 0 and 90°
Volume scan duration	200 s (3 min, 20 s)
Spatial resolution in range	500m ( $\pm 10$ m) & 1,000 m ( $\pm 20$ m)
in azimuth	1.0°
in elevation	from 0 to 85° (with 18 angles)
Rotation speed of antenna	5-6 rotation/minutes

Information on methods to calibrate the radar in absolute terms are unfortunately not available. In principle, one could check the calibration for the dual-wavelength radar by comparing reflectivity estimates on small targets (most likely in the Rayleigh regime ( $\pi D/\lambda \ll 1$ ) for both wavelengths, where  $D$  is hydrometeor diameter and  $\lambda$  is radar wavelength) close to the radar (to minimize attenuation loss at X-band), where  $Z$  values should be matched at the two wavelengths. Our checks on the literature suggest that this has been a missed opportunity for this radar.

To gain further information on the radar reflectivity calibration, all available 3D CAPPI files were searched for the maximum reflectivity value for each storm day. The search method covered an area of 14,400 km<sup>2</sup> centered on the radar and involved all CAPPI altitudes. The maximum reflectivity values are included in Table 3 which summarizes all storm dates investigated in the present study. It is noted that maximum values frequently attain the 50 dBZ level, with one value reaching 60 dBZ (for the 18 September 2018 storm). These large values are in line with other radar measurements in mountain thunderstorms (Dye et al., 1989; Lhermitte & Williams, 1984; Moore, 1965; Williams, 1990) and suggest that the MRL-5 radar is not reading low in reflectivity, and that the more modest values documented at the times of TGEs in Section 3 of this paper are real.

## 2.6. Thermodynamic Soundings

The temperature structure of the atmosphere is a key consideration in this study, given the cumulative evidence for a temperature-dependent tripole structure in thunderstorms. Thermodynamic soundings at 0 Z from the UGEE station (# 37,789, with latitude 40.21 N, and longitude: 44.48 E) in Yerevan, Armenia (Figure 2) and available from the University of Wyoming website (<http://weather.uwyo.edu/upperair/sounding.html>) have been used to document the environmental temperature structure on all days for the selected case studies here. This sounding site is unusual in making only one sounding per day at 0 UT (4 a.m. local time). Here we are assuming that the temperature structure aloft over Yerevan is representative of the profile in the vicinity of the Aragats station. Polynomial fits to the soundings have been implemented to establish altitude/temperature relationships.

Following the suggestion of one reviewer, additional tests were undertaken to justify the use of the Yerevan soundings at 4 a.m. local time to make in situ temperature assignments (below 0C) to the profiles of maximum radar reflectivity on the same day as the TGEs discussed in Section 3. In the first test, the sounding temperature at the respective altitudes of two elevated surface stations (Nor Amberd at 2,000 m MSL and Aragats at 3200 m MSL) were compared with simultaneous station measurements. These comparisons showed mean differences of about 2 C at Aragats and 1 C at Nor Amberd, with the sounding consistently “warmer” than the surface stations. This led us to hypothesize that the systematic differences were due to the nighttime radiative cooling at the surface sites, and that opposite differences would be documented in hypothetical daytime soundings due to surface heating in daytime. As a better test of that idea, daytime (4 p.m.) and nighttime (4 a.m.) soundings at Altenstadt, Germany (Station ID 10954), 39 km from the Zugspitze surface station whose altitude (2,960 m MSL) is similar to Aragats were examined. These comparisons showed that the sounding was consistently “warmer” than the Zugspitze (by ~2 C) in the nighttime comparisons but “cooler” than the surface site (by ~2 C) in the daytime soundings, consistent with the working hypothesis. These results show that while differences in temperature were noted, the results were largely local effects and likely did not impact the accuracy of the temperatures aloft from the soundings.

A final test was carried out with the daytime and nighttime soundings at Altenstadt by comparing temperatures obtained in the two sounding sets at a MSL altitude of 6.0 km (near the expected altitude of the main negative charge center of the tripole structure) on the same days. These results showed a mean temperature difference of ~1 C. This finding is in keeping with the general notion that diurnal variations in temperature aloft are small, lending further confidence to our decision to take the Yerevan 4 a.m. temperature as being representative over Aragats at other times on the same day as those selected for the surface-based TGE analyses.

## 3. Results

### 3.1. Procedure for Capturing TGE Events

A consistent procedure was followed in the identification of all TGEs in this study. First, concurrent time series records of the surface electric field and the collocated gamma ray flux at the Aragats observing station (hereafter



**Table 3**  
Summary of Information on the Working Collection of Thunderstorm Ground Enhancements (TGEs) for This Study

Event date	Time (LT)		STAND 1 cm			SEVAN (upper 5cm)			E field at TGE max (kV/m)	Temp. (°C)	Max of cloud top by radar (km)	Max dBZ within 14400 km <sup>2</sup>	N of CAPPIs checked for max dBZ
	Storm beginning	TGE	Duration (min.)	Intensity (%)	STDEV (σ)	Duration (min.)	Intensity (%)	STDEV (σ)					
1st category: cases in Positive field													
May 11, 2015	13:10	13:45	12	14.8	20.7	13	7.2	11.8	29.5	7	8	42.7	17
April 28, 2016	06:03	06:36	24	14.2	21.7	-	-	-	34	0.39	10	45.2	14
June 10, 2016	15:30	16:14	55	3.0	5	30	1.8	3	27.4	4.9	11	56.9	29
May 26, 2017	20:30	20:49	7	7.1	10.5	10	2.3	3.8	31.9	2.8	13	52.9	18
May 4, 2018	12:40	13:41	8	13.5	23.4	10	5.7	8.3	30.1	4.2	9.5	50.6	44
May 4, 2018	14:01	14:05	6	19.2	32	9	5.3	8	36.1	4.2	9	50.6	44
May 9, 2018	15:14	15:40	9	22.0	34.5	9	5.3	8.4	17.4	0.8	10	38.5	9
May 30, 2018	05:10	05:26	6	77.8	133	6	42.2	92	37.5	2.4	12	52.3	9
May 30, 2018	12:10	12:31	8	6.5	16	5	4.3	6.5	26.5	5.1	8.5	49.6	25
May 29, 2018	21:50	22:18	11	3.2	6.3	-	-	-	28.4	4.1	11	53.5	16
June 14, 2019	21:12	21:58	8	8.5	19	5	4.8	6.8	20.1	7.8	9.5	43.2	10
2nd category: cases in Negative field													
May 4 2016	22:40	23:03	21	20.5	39	6	7.5	12.3	-21.5	-0.6	8.5	36.5	10
May 4 2018	14:29	14:35	18	49.3	80	16	12.0	20	-29.2	4	9	50.6	44
May 23 2016	18:40	19:35	15	14.2	18.3	5	2.7	4.3	-21.9	4.3	10	44.7	12
June 11 2016	14:30	15:40	140	13.8	40	12	2.6	5.7	-32.6	5	13	53.8	30
May 6 2017	15:42	16:43	24	36.2	66	14	6.8	9.8	-33.6	1.8	10.5	48.1	18
June 1, 2017	07:47	08:23	9	1.1	19	8	1.5	4	-33	2.6	9	41.3	14
June 2 2018	21:40	22:32	10	43.1	85	10	11.6	16.9	-22.8	2.2	13.5	54.5	23
Sep. 18 2018	18:10	18:53	110	6.0	11.6	-	-	-	-29.2	5.2	13.5	60	18
May 14 2017	18:40	19:13	5	11.8	16	5	3.9	2.7	-37.7	2.7	10	45.8	15
3rd category collapsing: cases													
May 7 2017	13:35	13:56	18	25.1	48	11	2.4	3.8	-27.5	0.2	11	49.8	10
July 31 2017	18:50	20:09	105	26.9	39	6	4.0	6.5	-23.8	14.2	14.5	57.4	26
June 8, 2018	13:35	15:14	24	8.2	13.4	16	3.3	6.3	0	7.1	13	51.6	33
June 17 2018	13:50	14:53	150	8.0	15.3	-	-	-	-27	7.7	11.5	59.2	26
August 10 2018	16:35	17:35	107	9.0	22	-	-	-	-30.4	11.3	11.5	42.9	21
August 27 2018	18:00	18:37	120	8.5	13.6	-	-	-	-16.5	12.3	12	55.3	14
Sep. 18 2018	16:00	16:39	120	7.8	20.3	-	-	-	-14.5	8.3	13	50.1	13
June 14 2020	22:05	23:41	5	32.5	54	6	14.8	25	-17.7	7.7	10	45.4	27
May 18 2016	15:00	16:01	25	8.5	13.7	10	2.3	3.5	-25.8	1.1	11	57.7	24
May 23 2016	14:25	15:14	65	9.9	17	7	3.5	5.7	-18.3	5.5	12.5	52.9	18
October 5, 2015	07:50	08:08	7	12.2	29.2	6	6.0	10.19	27.4	1.6	10.5	50.9	27

Note. As shown in the table, we have registered 12 TGE events when near surface electric field was positive, 9 TGE events in negative field, and 10 TGE cases when we have a collapsing storm.

referred to simply as “Aragats” in the text) were examined for strongly correlated behavior. Generally speaking, the most pronounced anomalies in gamma ray flux occurred near the time of maximum field magnitude, of both polarities, as our selected examples will clearly show. When the field polarity indicated a dominant positive/negative charge overhead, the event was labeled a positive/negative TGE.

Once a candidate TGE was identified, the radar data were then consulted. Volume scan radar data were retrieved from the MRL-5 S-band archive to look for convective developments that appeared to coincide with the maxima in the surface electric field. The collection of all cases with well-defined TGEs and with accompanying radar data is included in Table 3. This Table also includes durations and intensities of TGEs on both the STAND1cm and SEVAN detectors, the maximum surface electric field and polarity, and various meteorological parameters (surface temperature, pressure, maximum radar height, and peak wind speed). From this larger collection of categorized cases, three best-defined cases each of “positive” TGEs and “negative” TGEs with stable vertical development in the radar observations were selected for detailed presentation (Sections 3.2 and 3.3). A third classification showing the rapid collapse of the storm was also identified in the “positive” TGE category and two cases were drawn from Table 3 for detailed presentation (Section 3.4). The implicit assumption in this search was that the convective electrification was precipitation-based and that the dominant precipitation type was graupel. This assumption is based on the overwhelming evidence for a thunderstorm electrification process based on collisions between graupel and ice crystals (Bateman et al., 1999; Marshall & Stolzenburg, 1998; Takahashi, 1978). Given that graupel is the dominant solid-phase hydrometeor in ordinary thunderclouds, radar is particularly well suited to identifying new regions of growth because the radar reflectivity depends on the sixth power of the graupel diameters (e.g., Battan, 1973). The other important consideration in the radar analysis was the proximity of the inferred convective development to the surface electric field measurement. For simple dipolar charge structures, the electric field is expected to fall off like  $1/R^3$ , where  $R$  is the distance to the convective feature. Accordingly, attention was focused on the development of radar reflectivity directly overhead and at a close slant range (<3 km) from the electric field measurement.

Given the abundant evidence for the tripolar electrical structure of ordinary thunderclouds (Bruning et al., 2007; Kuettner, 1950; Li et al., 2020; Mansell et al., 2010; Simpson & Robinson, 1940; Simpson & Scrase, 1937; Williams, 1989; Zheng et al., 2018), and with individual charge center heights tied to in situ temperature (Jacobson & Krider, 1976; Krehbiel, 1981, 1986; Kuettner, 1950; Simpson & Robinson, 1940; Simpson & Scrase, 1937), the most important consideration in interpreting the radar data pertained to the vertical development of the reflectivity in the volume scan data. Vertical profiles of maximum reflectivity at any given altitude are an important characteristic of the TGE cases examined.

A common finding with all the case studies addressed below is that the new convective growth, likely orographically induced, is occurring in the presence of debris cloud from earlier convection. This is evident from both the all-sky camera observations (not shown) and the radar observations. The likelihood of pre-glaciated conditions will become an important aspect of the interpretation of these remarkably electrified small clouds.

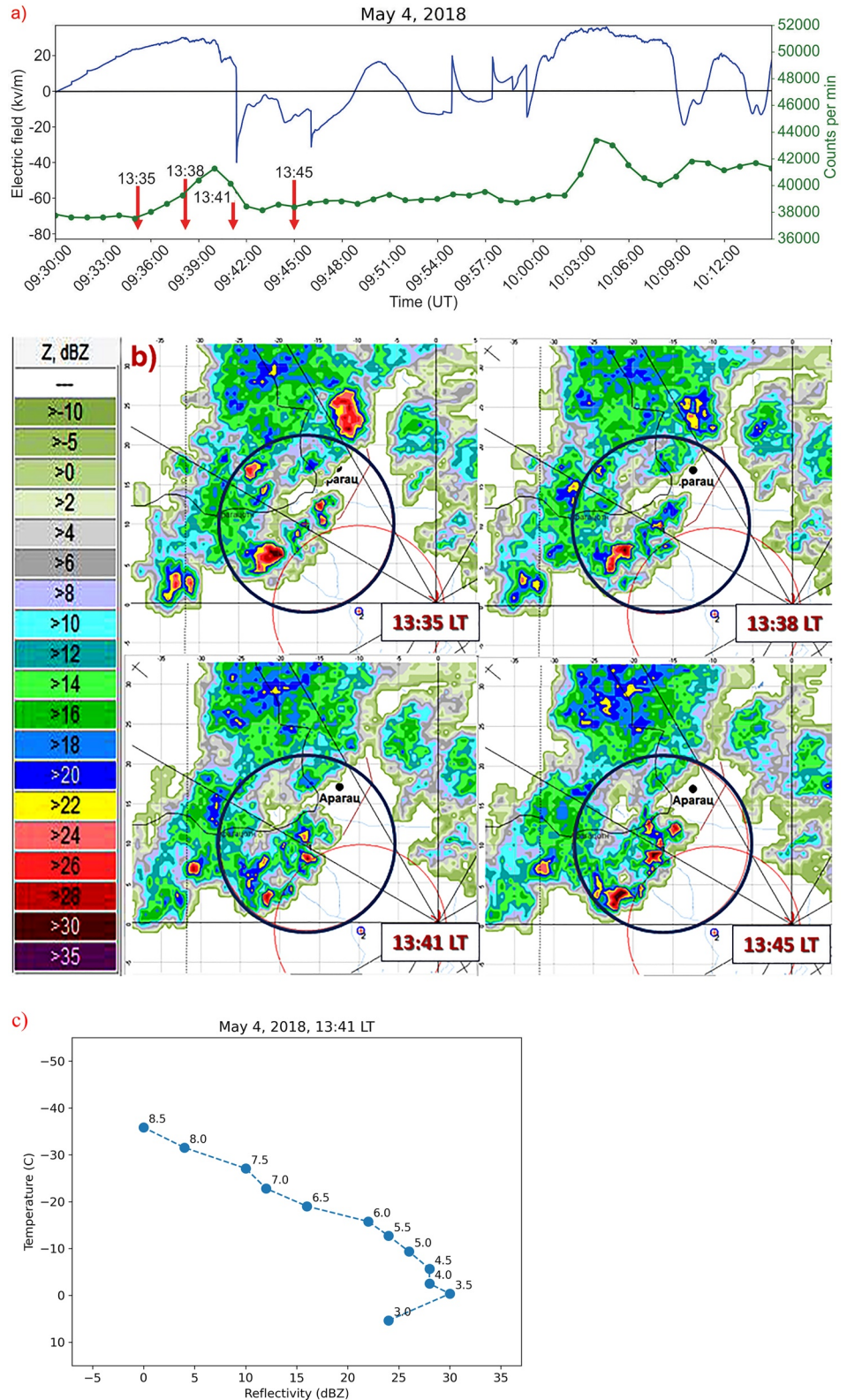
### 3.2. Selected Case Studies for Positive TGE Events Linked With Shallow Convection

#### 3.2.1. 4 May 2018

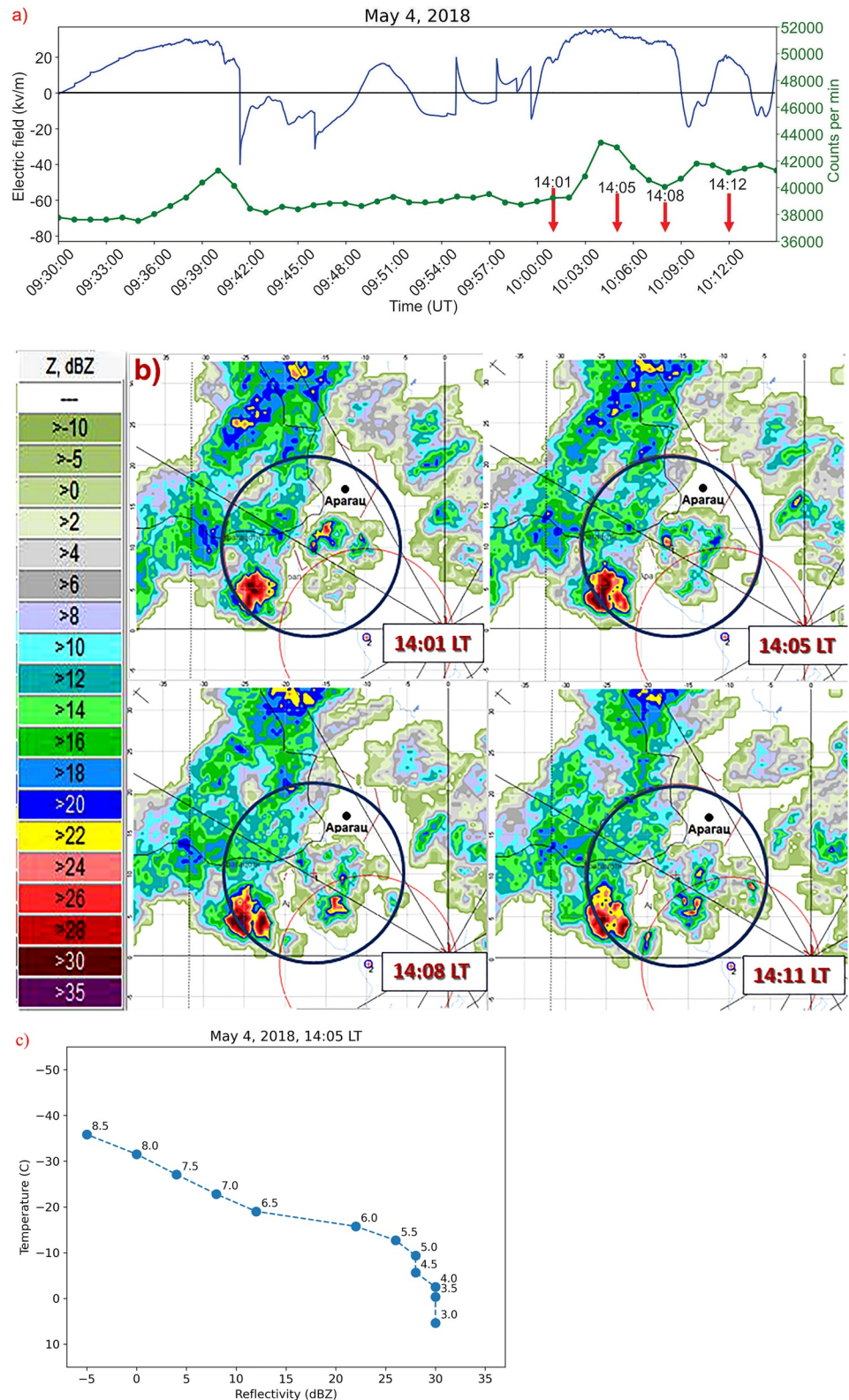
On this date, two positive TGEs were observed in fairly quick succession, 25 min apart. Figures 4a and 5a show the respective E field and gamma ray records. Both TGEs are clearly associated with strong positive excursions in the electric field, to values exceeding 30 kV/m. Four radar volume scans were available for each event. In both cases, the conspicuous maxima in particle flux are nearly coincident with the maxima in electric field, at 0940 UT (1340 LT) and 1004 UT (1404 LT), respectively. No evidence is seen for large discontinuities in electric field in the buildups to the TGE times that might be attributable to lightning. The two TGE events will now be discussed in turn.

Figure 4b shows the sequence of four radar CAPPIs at an altitude of 6 km MSL ( $T = -15.7^\circ\text{C}$ ) and corresponding to the four times marked by vertical red arrows for the first event on this day. Circles superimposed on all radar CAPPIs have 23 km diameters and are centered on the Aragats surface observations of electric field and gamma rays. An elongated clustering of small cells is evident, with a NE/SW orientation. New cell growth is evident directly over Aragats at 0935 UT (1335 LT) with a maximum area at 0938 UT (1338 LT) as the strong positive E field is increasing. Two cells with reflectivity reaching 30 dBZ are visible in the fourth CAPPI, one north and one south of Aragats and within 1–2 km. It is reasonable to assume that the electrification in these cells is responsible for the growth of the positive E field and the formation of the positive TGE at the ground.

Figure 4c shows the profile of maximum CAPPI reflectivity over Aragats at the time of the third CAPPI (0941 UT (1341 LT)), and closest to the time of the peak gamma ray flux at the surface. Every vertical profile of maxi-



**Figure 4.** Thunderstorm Ground Enhancements on 4 May 2018, with radar start time at 13:35 LT. (a) time series of surface electric field and gamma ray flux, (b) time sequence of four radar Constant Altitude Plan Position Indicator (CAPPI) at an altitude of 6 km MSL ( $T = -15.7$  (c)), (The superimposed circles with diameters of 23 km are centered on the Aragats surface observations). (c) vertical profile of maximum CAPPI reflectivity over Aragats at 1341 LT.



**Figure 5.** Thunderstorm Ground Enhancements on 4 May 2018 with radar start time at 14:01 LT. (a) time series of surface electric field and gamma ray flux, (b) time sequence of four radar Constant Altitude Plan Position Indicator (CAPPI) at an altitude of 6 km MSL ( $T = -15.7^{\circ}\text{C}$ ). (The superimposed circles with diameters of 23 km are centered on the Aragats surface observations). (c) vertical profile of maximum CAPPI reflectivity over Aragats at 1405 LT.

imum reflectivity is produced by finding the largest value of reflectivity (dBZ) within 3 km of the vertical line centered on the Aragats surface observations. This profile shows a maximum of 22 dBZ at 6 km ( $T = -15.7^{\circ}\text{C}$ ) and a rapid decline at a greater altitude. This reflectivity profile is weaker than is typical for other active mountain thunderstorms (Dye et al., 1989; Raymond et al., 1991) in New Mexico, for example, Williams (1990) is a counterexample. A possible explanation for weaker reflectivity in these Aragats storms was considered earlier in the radar discussion in Section 2.5.

Figure 5b shows the sequence of four CAPPIs for the second positive TGE documented in Figure 5a, with red arrows marking the CAPPI times. Since this event is only 25 min later than the first, one sees reflectivity features here that are correlated with those in Figure 4b, especially the larger cell 7–8 km southwest of Aragats. But a new cell is evident at 1001 UT (1401 LT) directly over Aragats and this cell enlarges in the area and intensifies to 36 dBZ (with little apparent advection) by the second CAPPI at 1005 UT (1405 LT) which is the closest to the time of the TGE. By 1008 UT (1408 LT) the same cell is showing signs of decay at this altitude.

Figure 5c shows the profile of maximum reflectivity for the second volume scan at 1405 LT when the gamma ray flux is strongest. A reflectivity of 28 dBZ is evident at 4.5 km MSL ( $T = -5.7^{\circ}\text{C}$ ) altitude, and then the reflectivity declines markedly with altitude above 5 km MSL ( $T = -15.7^{\circ}\text{C}$ ). This weak profile is generally consistent with the absence of lightning, but the development of a positive electric field exceeding 30 kV/m (see also Figure 4) is remarkable.

### 3.2.2. 30 May 2018

This event was identified in an earlier study (Chilingarian, Hovsepyan, et al., 2018) and characterized therein as “one of the four largest TGE events observed on Aragats in the last decade” (133 Standard deviations in gamma ray flux on the STAND 1 detector, see Table 3). No radar analysis accompanied this earlier study, but the modest vertical development for this storm is entirely consistent with the other selected examples of positive TGEs.

Figure 6a shows the concurrent records of surface electric field and gamma ray flux, and shows a strong peak in the flux (at 0126 UT (0526 LT)) after the electric field transitions to positive polarity (dominant + charge overhead). Additional evidence in the E field record is noted for a lightning discharge during this transition and a second discharge nearly coincident with the time of maximum flux. The total duration of the flux enhancement is less than 4 minutes, in keeping with a convective time scale for these events.

Figure 6b shows a time sequence of six CAPPIs all at an altitude of 5 km MSL ( $T = -5.3^{\circ}\text{C}$ ). A contiguous line of convection, only ~2 km wide, oriented northwest/southeast is advancing toward Aragats from the southwest as the foul weather field (Figure 6a) increases in magnitude, through the times of the first four CAPPIs. By the time of the fifth and +TGE coincident CAPPI (0126 UT (0526 LT)), this convective line is directly over Aragats, nearly coincident with the maximum value of positive electric field. In the sixth and final CAPPI (0130 UT (0530 LT)) a major reduction in reflectivity is noted and the electric field has reverted to negative polarity. This sequence suggests that a lower positive charge has fallen out of the storm on radar-detected precipitation.

The vertical profile of maximum reflectivity extracted from the volume scan at 0126 UT (0526 LT) is shown in Figure 6c. Maximum values are 25–30 dBZ up to an altitude of 5 km MSL ( $T = -5.3^{\circ}\text{C}$ ). Above this altitude, the reflectivity declines sharply, similar to the other selected examples of +TGE storms. So, despite the exceptional nature of this event noted earlier (Chilingarian, Hovsepyan, et al., 2018), the radar characteristics are in line with the other examples of positive TGE storms.

## 3.3. Selected Case Studies for Negative TGE Events Linked With Deep Convection

### 3.3.1. 11 June 2016

This storm exhibiting a well-defined negative TGE is decidedly larger and more electrically active than any of the storms producing positive TGEs discussed earlier. Figure 7a shows simultaneous records of electric field (black trace) and gamma ray flux (blue trace). Numerous (many per minute) discontinuities associated with lightning flashes are evident in the early part of the record when the prevailing field is positive polarity. Six red vertical arrows showing the sampling times for consecutive radar volume scans are also included. The initially positive field trends negative for the first time near the second volume scan (1141 UT (1541 LT)) and then recovers quickly to positive polarity, before transitioning to negative electric field and a nearly coincident upsurge in

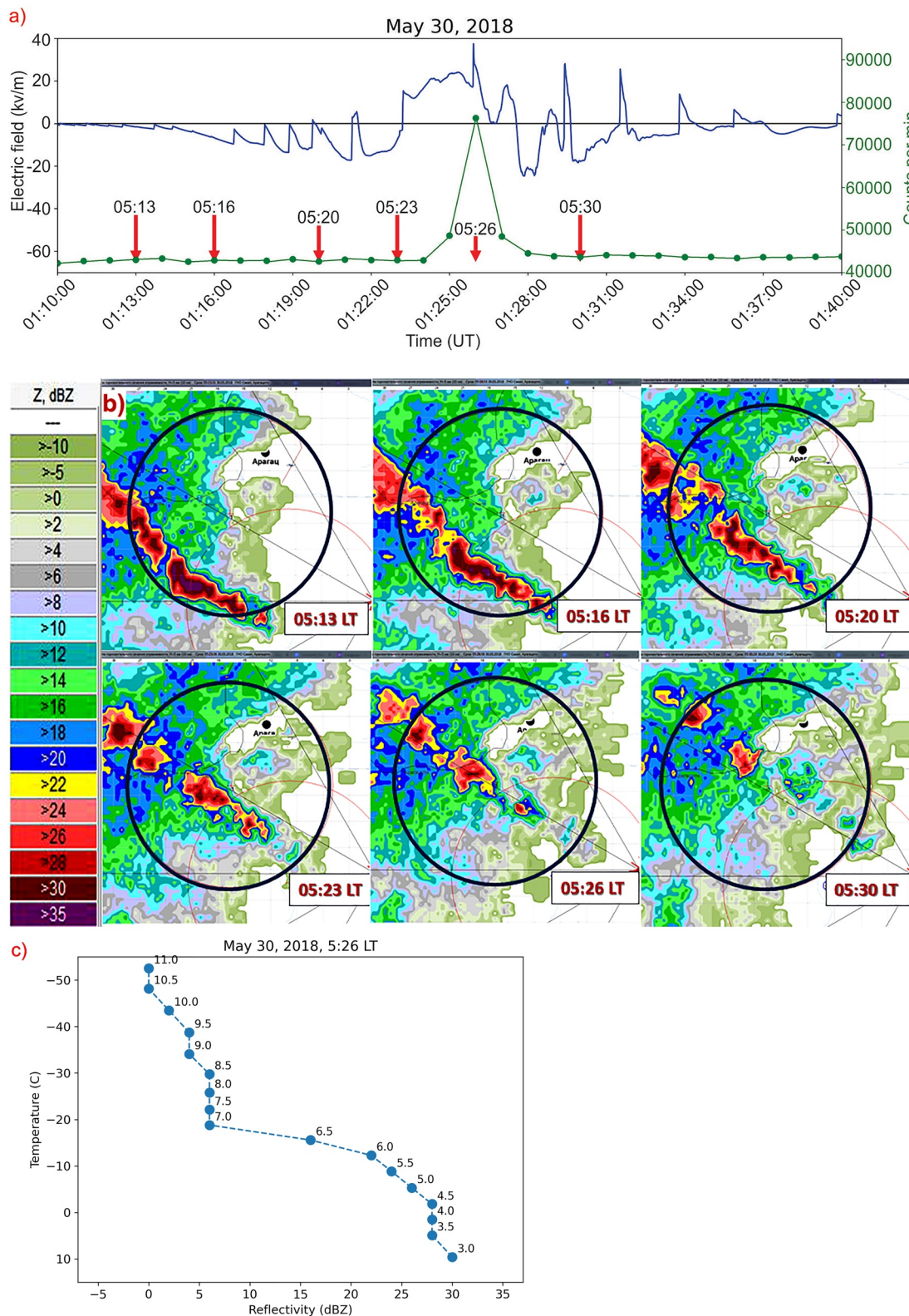


**Figure 6.** Thunderstorm Ground Enhancements on 30 May 2018 with radar start time 0513 LT (a) time series of surface electric field and gamma ray flux, (b) time sequence of six Constant Altitude Plan Position Indicator (CAPPI) all at an altitude of 5 km MSL ( $T = -5.3^{\circ}\text{C}$ ). (The superimposed circles with diameters of 23 km are centered on the Aragats surface observations). (c) vertical profile of maximum CAPPI reflectivity extracted from the volume scan at 0126 UT.

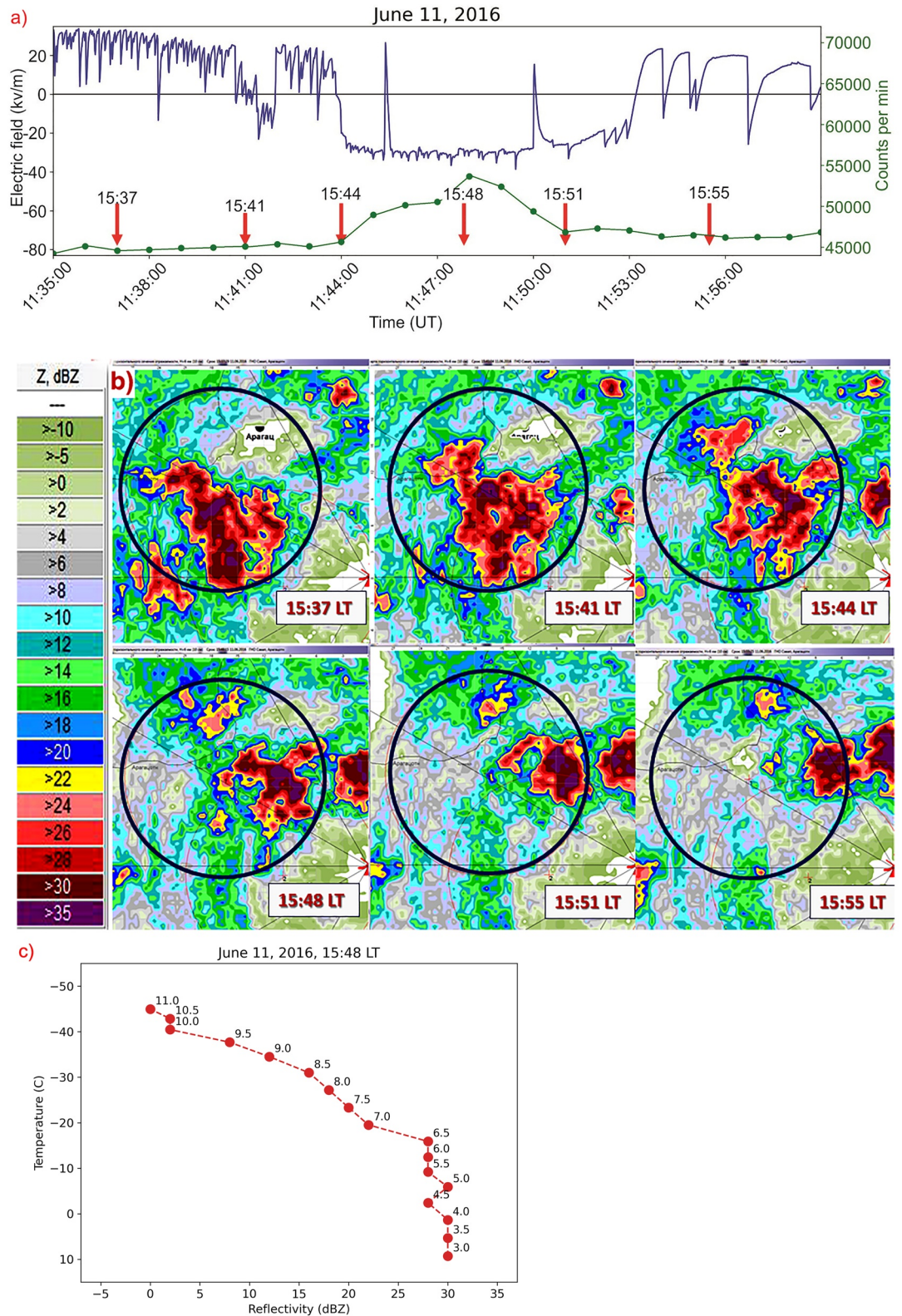


**Figure 7.** Thunderstorm Ground Enhancements on 11 June 2016 with radar start time 1537 LT, (a) time series of surface electric field and gamma ray flux, (b) time sequence of six Constant Altitude Plan Position Indicator (CAPPI) all at an altitude of 6 km MSL ( $T = -12.5^{\circ}\text{C}$ ), (The superimposed circles with diameters of 23 km are centered on the Aragats surface observations). (c) vertical profile of maximum CAPPI reflectivity at 1548 LT.

gamma flux near 1143 UT (1543 LT) which is then sustained for ~10 min until 1153 UT (1553 LT) when the field reverts again to positive polarity.

Many small discontinuities in the electric field record characterize this negative TGE period, but also two large field changes indicating an abrupt lowering of negative charge by lightning, one coinciding with the increase in the TGE gamma ray flux and the other accompanying the decrease in flux toward the end of the event. An expanded view of the large field changes can be seen in Figure 12c.

Figure 7b shows the sequence of six radar CAPPIs (at an altitude of 6 km MSL ( $T = -12.5^{\circ}\text{C}$ )) at the six times indicated in Figure 7a by red arrows. The horizontal extents of the strong reflectivity features here are 3–5 times larger than the examples pertaining to the positive TGE events shown earlier. A consistent pattern of advection of the cellular features from the west-southwest across Aragats is evident over the CAPPI time sequence. In the initial CAPPI (1137 UT (1537 LT)) a 40+ dBZ core is evident 2–3 km southwest of Aragats. By the third CAPPI (1144 UT (1544 LT)) a local maximum in reflectivity is centered on Aragats, just at the outset of the TGE. In the fourth CAPPI (1148 UT (1548 LT)) and close to the time of the maximum gamma ray flux, Aragats is on the rear edge of the reflectivity maximum. For the fifth and sixth CAPPIs, the storm has moved beyond Aragats by a few kilometers.

The evidence for large negative charge removal with this storm overhead and small positive charge removal between the time of the fifth CAPPI and into the sixth CAPPI together support the presence of a strong (upper) positive dipole structure for this storm.

Figure 7c shows the vertical profile of maximum reflectivity at any given altitude extracted from the radar volume scan at 1151 UT (1551 LT) closest to the time of maximum gamma ray flux in the negative TGE. This profile is more strongly developed than those shown in conjunction with the positive TGEs documented earlier, with a profile maximum (25–30 dBZ) reaching an altitude of 6.5 km MSL and an environmental temperature of  $\sim -16^{\circ}\text{C}$ . The profile is substantially stronger than positive TGE cases at higher levels as well, with 10 dBZ extending to 9–9.5 km MSL ( $T = -34.5^{\circ}\text{C}$ ) in this storm.

### 3.3.2. 6 May 2017

This storm case demonstrates how a laterally compact reflectivity feature (unlike the previous example) can produce a negative TGE so long as the vertical development is sufficiently strong. Figure 8a shows the variation of surface electric field (black) and gamma ray flux (blue) for a ~50 min period on 6 May 2017. Vertical red arrows again show six times of radar volume scans. An active lightning period ( $\sim 1$  flash/min) and positive electric field precede the time of the first volume scan. The conspicuous “negative” TGE in gamma ray flux is nearly coincident with the strongest negative field ( $>30$  kV/m) for the entire storm day, close to the time of the third volume scan (1243 UT (1643 LT)).

A large discontinuity in electric field (1243 UT (1643 LT)) associated with a lowering of negative charge accompanies the declining phase of the gamma ray flux in the TGE.

Figure 8b includes the sequence of six CAPPIs (at an altitude of 6 km MSL) at times indicated by red vertical lines in Figure 8a. Scattered convective cells are present both east and west of Aragats. The rapid decay of reflectivity overhead from the first to the second CAPPI is consistent with the decay in electrical activity evident in Figure 8a. But a tiny cell in the new development is seen nearly overhead in the second CAPPI. By the time of the third CAPPI (1243 UT (1643 LT)), this cell has enlarged considerably and had attained a reflectivity exceeding 25 dBZ. The maximum cell diameter is only 3–4 km at this time. This development closely coincides with the maximum gamma ray flux in the TGE. By the time of the fourth CAPPI (1246 UT (1646 LT)), the overhead cell has already decayed in the area and in reflectivity, and the gamma ray flux is no longer anomalous. Other cell developments are visible nearly overhead in the fifth and sixth CAPPIs and may be linked with a secondary development of gamma ray flux in Figure 8b that maximizes at 1252 UT (1652 LT) and between the times of these two CAPPIs.

Figure 8c depicts the vertical profile of the maximum reflectivity extracted from each altitude of the radar volume scan that coincides with the peak TGE at 1241 UT (1641 LT). Maximum values are 30 dBZ, diminished to 20 dBZ at 7 km MSL (where  $T = -26^{\circ}\text{C}$ ) and then a more rapid decline but with detectable reflectivity to 9.5 km MSL altitude. Though not a strong profile in the context of ordinary active thunderstorms, this profile is notably



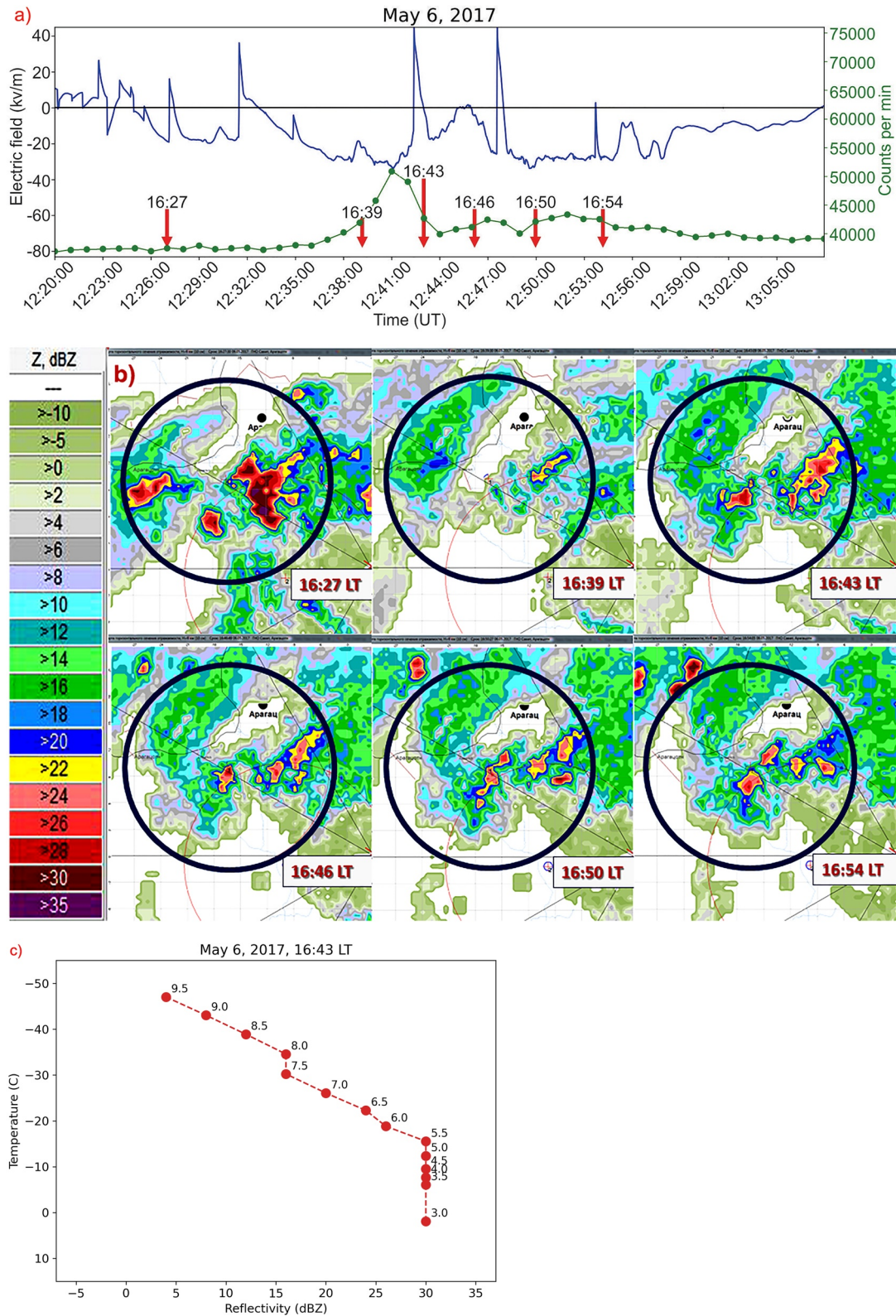


**Figure 8.** Thunderstorm Ground Enhancements on 6 May 2017 with radar start time 1627 LT. (a) time series of surface electric field and gamma ray flux, (b) time sequence of six Constant Altitude Plan Position Indicator (CAPPI) all at an altitude of 6 km MSL ( $T = -18.8^{\circ}\text{C}$ ), (The superimposed circles with diameters of 23 km are centered on the Aragats surface observations). (c) vertical profile of maximum CAPPI reflectivity at 1643 LT.

stronger than the profiles documented for the positive TGE cases, despite the small reflectivity area involved with the convective development.

The TGE on this day was previously considered by Chilingarian, Hovsepyan, et al. (2018) as an example of how a terminating lightning flash could abruptly reduce the gamma ray flux (documented in Figure 12d) at the surface beneath the storm. The following documentation brings the S-band radar data to this case.

### 3.3.3. 1 June 2017

This final example of a negative TGE case is similar to the previous one in showing highly localized growth of radar reflectivity in the mixed-phase region directly over the Aragats measurements, but without production of large-scale lightning, at least in the initial growth of the TGE. Figure 9a shows simultaneous records of the electric field (black) and gamma ray flux (blue) at Aragats. The six vertical red arrows show the times of the radar volume scans, with the third scan closest in time to the conspicuous TGE maximum at 0423 UT (0823 LT). This strong excursion is a 21-standard-deviation event on the STAND 1 cm detector (Table 3). The electric field lacks any indication of abrupt discontinuities, even as the field reverses polarity from positive to negative field in the interval 0419 to 0422 UT (0819–0822 LT) as the gamma ray flux intensifies.

Figure 9b shows the sequence of six CAPPIs, each at an elevation of 6 km MSL ( $T = -20^{\circ}\text{C}$ ), corresponding to the six red arrows shown in Figure 9a. The CAPPIs are dominated by a few scattered cells (with diameters of a few kilometers), all within the 23 km-diameter circle centered on Aragats, prior to the time of the TGE. The smallness of the cells is consistent with the evidence for an absence of lightning in the E field record. One small cell with reflectivity reaching 30+ dBZ is dead-center over Aragats in the first CAPPI. New cell growth is evident to the east-northeast of this initial cell in the second CAPPI at 0419 UT (0819 LT) concurrent with the strong excursion of an electric field to negative polarity, indicative of the growth of dominant negative charge overhead. This same cell shows intensification to 31 dBZ in the third CAPPI and further enlargement of the 25 dBZ reflectivity contour in the fourth CAPPI at 0426 UT (0826 LT). By the time of the fifth CAPPI (0430 UT (0830 LT)), this nearest cell to Aragats had decayed, consistent with the decline in the gamma ray flux. The decay of this cell continues into the final (sixth) CAPPI, though other smaller cells remain and may be important for the sustenance of the strong negative E field remaining after the gamma ray flux declines.

Figure 9c shows the vertical profile of maximum reflectivity extracted from the volume scan closest in time to the peak gamma ray flux (0423 UT (0823 LT)). A reflectivity of 24 dBZ is sustained until an altitude of 6.5 km MSL ( $T = -25^{\circ}\text{C}$ ) and then declines at higher levels. Detectable reflectivity is still present above 9 km MSL, in contrast to like profiles for the positive TGE cases presented earlier.

Evidence has also been found for “negative” TGEs beneath deep debris clouds from earlier deep convection, and exhibiting radar reflectivity less than values typical for graupels ( $\sim 30$  dBZ). These events have not been treated here for lack of space but are deserving of further study.

## 3.4. Collapse of Deeper Storms: TGEs With Positive E Field

The observations described so far in this paper demonstrate a clear tendency for “positive” TGEs associated with shallow (i.e., “warmer”) storms and “negative” TGEs with deeper (i.e., “colder”) storms. The discovery of another set of positive TGE events associated with deeper storms appeared at first to contradict the main working hypothesis. However, when a more thorough Lagrangian analysis of several of these cases was undertaken to show the collapse of these storms in their arrival over the Aragats observation site, a more harmonious picture emerged. “Positive” TGEs remain linked with shallow vertical development.

The previously described (Section 3.3) TGE cases showed quasi-stable vertical development of reflectivity over the nominal five-minute duration of the TGE, and a single vertical profile of maximum reflectivity over the observation site (formally speaking, an Eulerian analysis of radar observations) was adequate to characterize the storm vertical development. To characterize the collapse of these initially deeper storms, we needed to follow the evolution of their profiles of maximum reflectivity in a period prior to their arrival at the Aragats observation site. This involved the identification of the main convective cell (or cell cluster) in successive CAPPI sets and at all CAPPI heights as the cell progressed from the west (and upslope given the elevated location of the observation site at 3,200 m MSL, as shown in Figure 2) over the observation site. Formerly speaking, this is a Lagrangian analysis, moving with the cell.

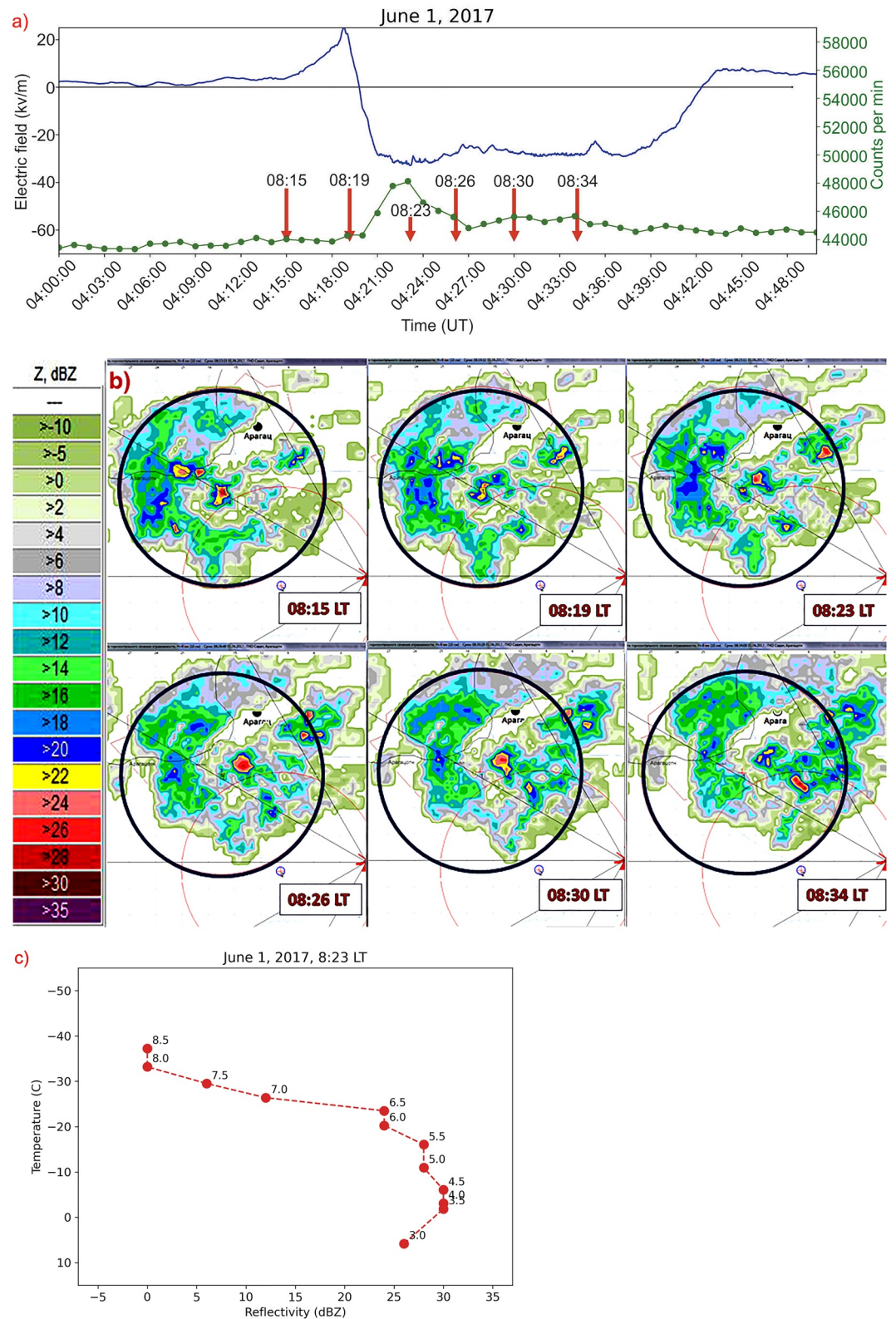


**Figure 9.** Thunderstorm Ground Enhancements on 1 June 2017 with radar start time 0815 LT, (a) Time series of surface electric field and particle flux, (b) time sequence of six Constant Altitude Plan Position Indicator (CAPPI) all at an altitude of 6 km MSL ( $T = -20^{\circ}\text{C}$ ) (The superimposed circles have diameters of 23 km). (c) vertical profile of maximum CAPPI reflectivity at 08:23 LT.

Two examples were selected for this systematic collapsing storm behavior (5 October 2015 and 8 June 2018), and similarities between the two cases will be noted. A time-height evolution of maximum reflectivity (Lhermitte & Williams, 1984) at every CAPPI height will serve as the main radar documentation in each case.

#### 3.4.1. 5 October 2015

Figure 10a shows simultaneous records of the electric field (black) and gamma ray flux (blue) at Aragats, just as in the earlier case studies. Times of radar volume scans used for this analysis is again shown with red arrows. Figure 10b also shows the evolution of maximum radar reflectivity in time-height format. Also shown in the bottom panel is a record of storm distance, including the range from field mill location to the maximum reflectivity value and the distances from both closest and furthest detectable reflectivity. The flash rate history based on the field changes in the field mill record is also shown (Figure 10c).

Specific features of the electric field record can be paired with specific features of the time-height reflectivity plot. In the time interval 0740–0800 LT, the storm is deepening as the electric field trends negative, indicative of a buildup of dominant negative charge in the main positive dipole region. Many field changes of the order of 1 kV/m in amplitude are consistent with the distance of  $\sim 13$  km to the storm core around 0755 LT. A modest peak flash rate of 2 flashes per minute is evident in the electric field record at 0754 LT when the radar cloud top height (0 dBZ threshold) is 11 km (MSL).

A transition from negative to positive electric field occurs at 0757 LT, suggesting a growing influence of the LPCC at a time that includes both the rapid collapse of the radar reflectivity aloft and the increased proximity of the main cell to the field observation site. Field changes with the same polarity as before are evident (at 0757 LT and 0759 LT), suggesting the presence of IC flashes in the main dipole of the storm that leaves orphaned the LPCC and thereby increase the magnitude of the positive field. Such field changes are conspicuous in this and other examples, and are appropriately called “tripole field changes”.

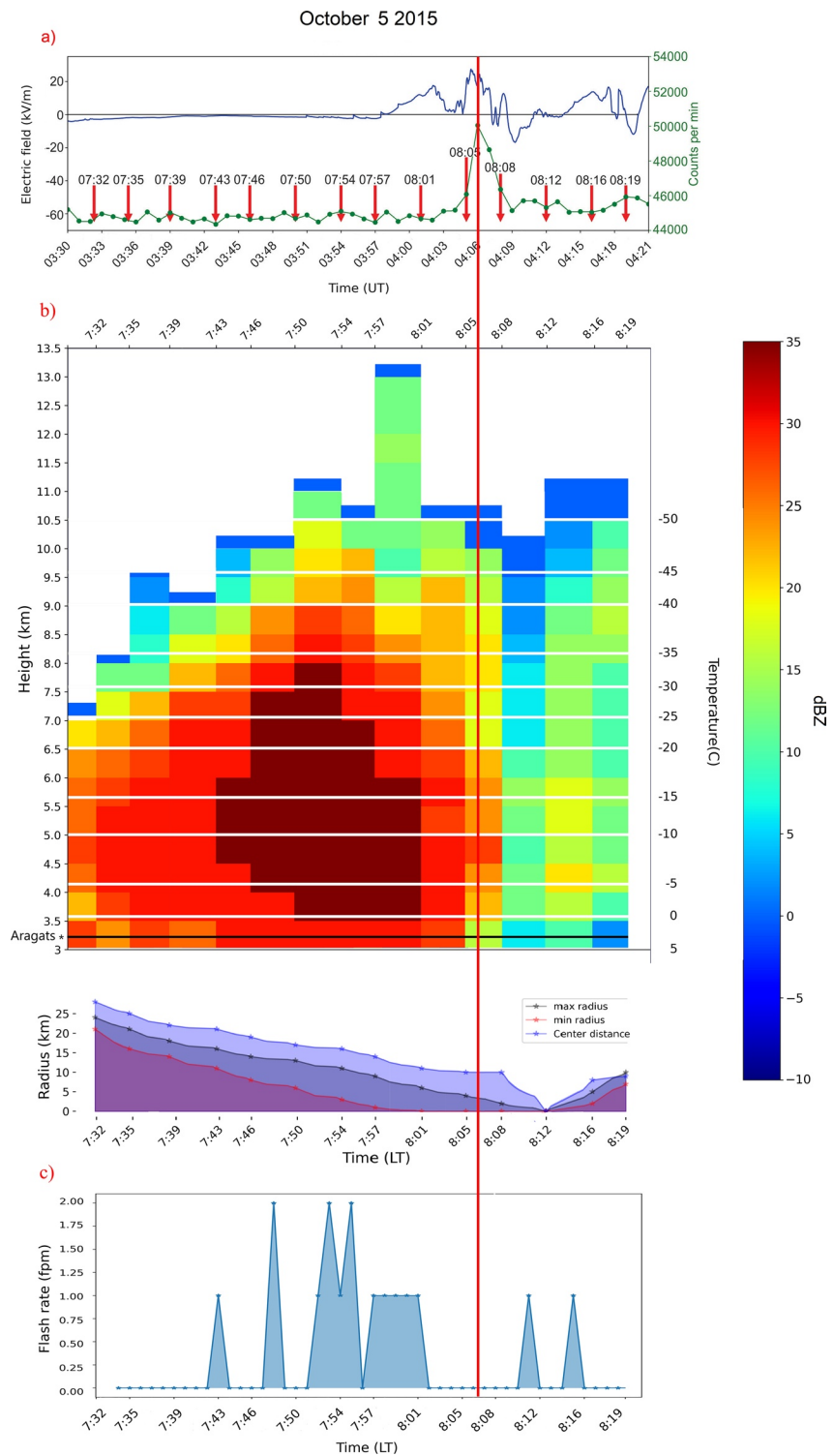
After a weakening of the magnitude of the positive field in the interval 0802–0804 LT, the magnitude again increases to its maximum value of the entire storm at 0805 LT, 1 min prior to the maximum gamma ray flux of the TGE (at 0806 LT). Both the collapse of the radar vertical development and the increased proximity of the main cell has continued to this juncture, consistent with the dominance of the LPCC in both the TGE and the behavior of the surface electric field.

Following the storm collapse and the disappearance of reflectivity  $>25$  dBZ, the electric field exhibits a strong excursion to opposite (negative) polarity, supporting the dominance of residual negative charge in the main dipole at this stage. The maximum negative field occurs at 0809 LT and both the anomalous TGE flux and all lightning flashes have ceased.

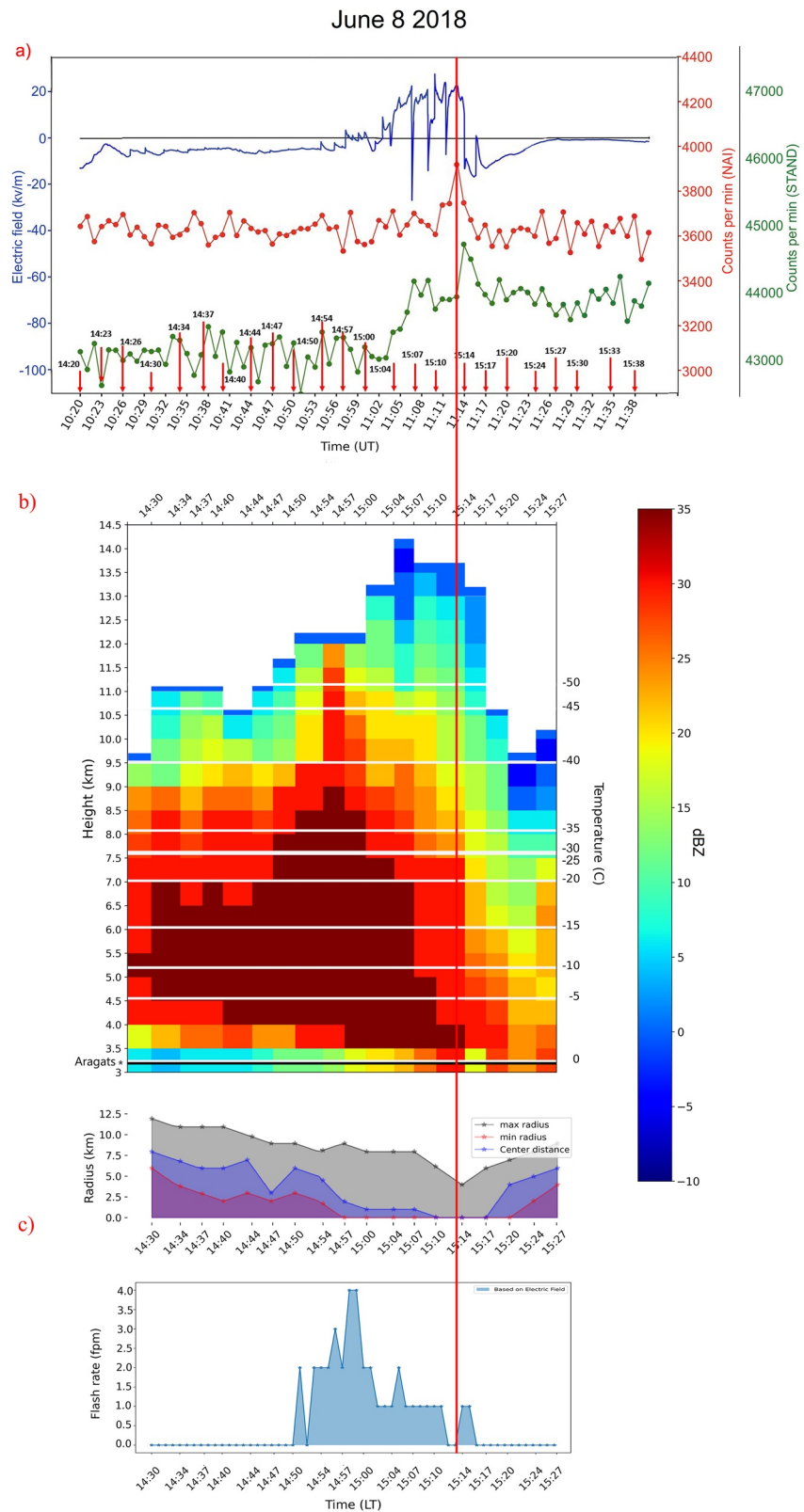
#### 3.4.2. 8 June 2018

Figure 11a displays simultaneous records of the electric field (black) and gamma ray flux (red, NaI detector and green, STAND1 detector). The time-height plot of maximum reflectivity, together with storm proximity information for 8 June 2018 in the same format as for the earlier 5 October 2015 case. Many similarities with the earlier collapsing storm will be noted below. This approaching storm is somewhat more complicated in that multiple cells (not shown) are involved, but a clear presence of a negative electric field is apparent (with a magnitude  $\sim 5$  kV/m) in this approaching-storm in the time interval up to 1502 LT. The maximum reflectivity in Figure 11b shows strong upward development to a maximum cloud top height of 12 km (MSL) at 1450 LT as the cells migrate toward Aragats from the west. Consistent field changes with positive polarity are evident in this time interval, consistent with IC flashes in the main dipole region, and also consistent with typical thunderstorm development elsewhere (e.g., Krehbiel, 1986). The peak flash rate in Figure 11c (1459 LT) occurs just after the peak vertical development.

The onset of the strong collapse of this storm is evident from 1450 LT through the time of the TGE at 1514 LT. The strong excursion from negative to positive E field is evident near 1504 LT during a notable diminishment of reflectivity in the temperature domain of the main dipole region ( $-10$  to  $-20^{\circ}\text{C}$ ) and the descent of (inferred) graupel into the temperature domain of the LPCR ( $0^{\circ}\text{C}$  to  $-10^{\circ}\text{C}$ ). Beginning at 1504 LT, lightning-associ-



**Figure 10.** Stacked plot with (a) time series of surface electric field and gamma ray flux, (b) time-height plot of maximum reflectivity and information on cell proximity, and (c) flash rate history, all for the collapsing storm on 5 October 2015. The red line is showing the peak time of the Thunderstorm Ground Enhancement.



**Figure 11.** Stacked plot with (a) time series of surface electric field and gamma ray flux (with two detectors), (b) time-height plot of maximum reflectivity and cell proximity information, and (c) flash rate history, all for the collapsing storm on 8 June 2018. The red line is showing the peak time of the Thunderstorm Ground Enhancement.

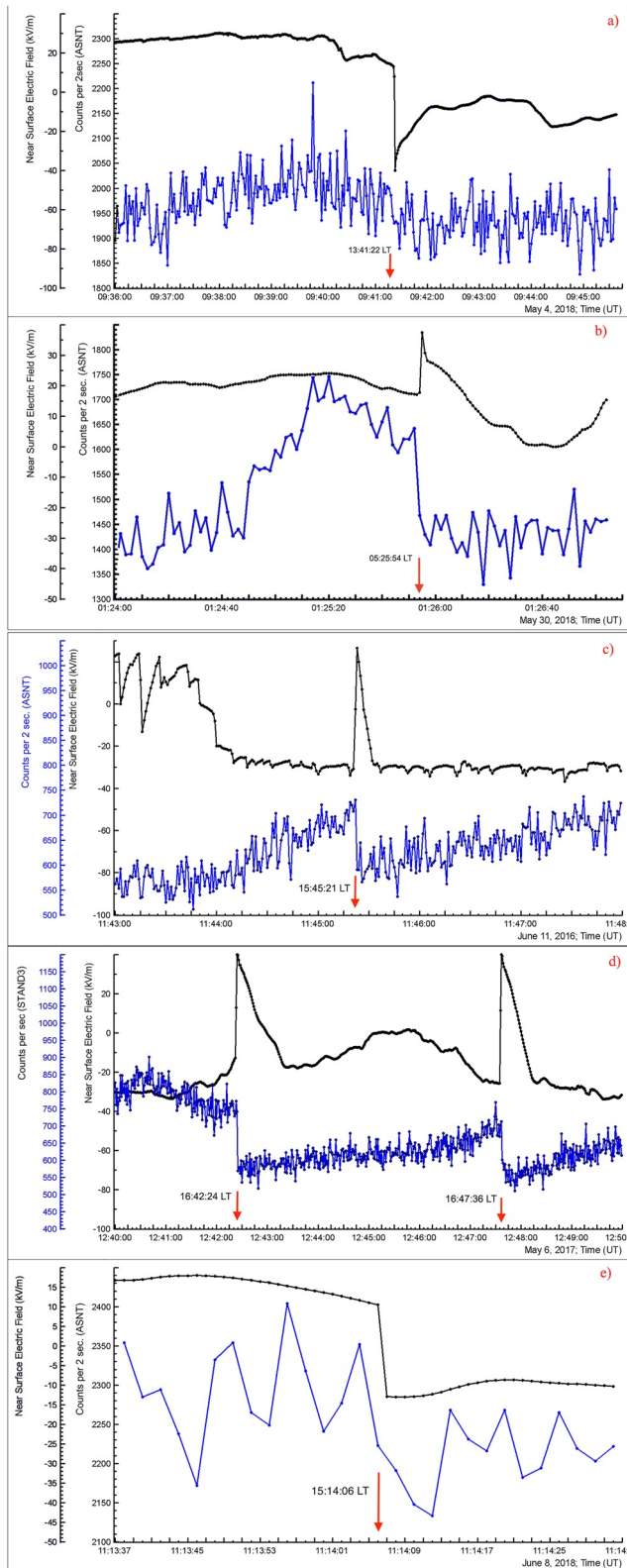


**Figure 12.** Terminating lightning in the electric field record and synchronous decreases in gamma ray flux for (a) 4 May 2018 (ASNT), (b) 30 May 2018 (ASNT) (c) 11 June 2016 (STAND) (d) 6 May 2017 (STAND) (e) 8 June 2018 (ASNT). Red arrows mark the times of the terminating flashes.

ated negative changes in the electric field are evident, plausibly caused by IC flashes in an active lower (inverted) dipole that diminishes the LPCC nearest the field mill on the ground.

As with the October 5 case, both the collapse and the increasing proximity of the main cell to the Aragats observation site appear to contribute to an increasing influence of the LPCC on the surface electric field and on the formation of the TGE.

By the time of the TGE at 1514 LT, the radar top has descended from a maximum of 14 km MSL at 1504 LT to a height of 9.5 km MSL, a total drop of 4.5 km. This evidence is consistent with the observations from other shallow storm cases showing “positive” TGEs, that the lower inverted dipole of the general tripole structure is playing a fundamental role in the downward acceleration of runaway electrons.

This 8 June 2018 case (and other cases on 7 May 2017; 17 June 2018 and 10 August 2018, not shown for lack of space) also illustrates the importance of the selection of gamma ray detector in the documentation of the TGE. Chilingarian (2018a) had earlier shown the importance of radon progeny as a source of enhanced gamma radiation in the proximity of Aragats storms. This radon source is physically distinct from the gamma radiation linked with the RREA process and electron runaway, which involves higher energy (>3 MeV gammas; see also Wada et al., 2021). Figure 11a, (red) shows the comparative behavior of electric field and gamma ray histories with the STAND1cm detector (with gamma ray response from 0.1 to 5 MeV) and a NaI #5 detector (>3 MeV response). The superimposed gamma response with the STAND 1 cm detector (Figure 11a, green) leaves the confused impression that the TGE maximum is occurring during the transition in the electric field from positive to negative polarity. But when the radon signal is removed and only the most energetic gammas are retained, the correspondence of TGE maximum with positive electric field is preserved. It is also apparent from Figure 11a that the relative change in count rate is greater when only the most energetic gamma rays are registered. This finding is consistent with the observations of TGEs in winter storms in Japan at sea level by Wada et al. (2021).

## 4. Discussion

### 4.1. Vertical Profiles of Radar Reflectivity for “Positive” and “Negative” TGEs

The physical distinction in the origin of TGEs in positive and negative electric fields is a central goal of this study. Figure 13 draws together the vertical profiles of maximum reflectivity for the six case studies previously discussed, three in the strong positive field and three in strong negative field. The Yerevan temperature soundings on the respective storm days were used to transform radar-based MSL altitude to environmental temperature, given the abundance of evidence in earlier studies that the charge accumulation zones in the vertical are temperature-dependent (see references in Introduction).

A clear distinction is evident in the respective profiles above the 0°C isotherm. The profiles for the “positive” cases decline markedly in the temperature interval  $-10^{\circ}\text{C}$  to  $-20^{\circ}\text{C}$  widely recognized as containing negatively charged graupel particles in ordinary thunderstorms. In contrast, the profiles for the “negative” cases exhibit order-of-magnitude stronger reflectivity throughout this region and extend to the tops of the measured storms.

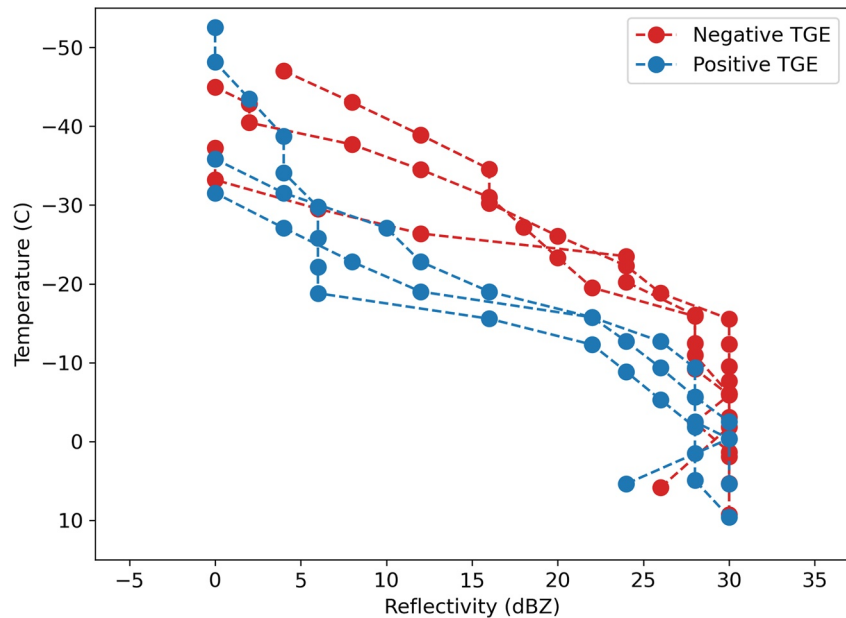


**Figure 13.** Collection of all six case study vertical profiles of radar reflectivity versus temperature.

Figure 1 illustrates the physical interpretation of the radar observations in Figure 13, in the context of the temperature-dependent tripole structure. Two distinct scenarios are shown in Figure 1, one for positive TGEs (left) and one for negative TGEs (right). The high field zone of downward electron acceleration is shown by the light red ellipse in both cases. The full tripole and “negative” TGEs are manifest when graupel collisions with ice crystals are active within the main dipole. This scenario may likely involve the action of a particle balance level (Atlas, 1966) with updraft ascent balanced by graupel fall speed (Lhermitte & Williams, 1985). Alternatively, this scenario may depend on the existence of a charge reversal temperature (Jayaratne & Saunders, 1984) within the main negative charge region where the relative dominance of negative space charge from cloud particles and from graupel particles changes with height within the main negative charge layer (Bateman et al., 1999; Marshall & Stolzenburg, 1998). The shallower inverted dipole is manifest when graupel collisions with crystals are most active at warmer temperatures. A legitimate question arises as to why the lower (inverted) dipole is suppressed in the full tripole when the reflectivity profile shows evidence for graupel in the lower dipole region. One possible explanation is the absence of ice crystals at warmer temperatures. And why then are crystals present in the case of the inverted dipole/“ positive” TGE scenario? It is possible that on Mt Aragats one has orographically forced upslope convective development with a pre-glaciated condition due to previous storm activity. The establishment of such conditions will require observational assets beyond what has been assembled for the present study.

The maximum values of reflectivity in all vertical profiles documented in Figure 13 are of the order of 30 dBZ. These values are modest in comparison with maximum reflectivity values (40–60 dBZ) known to exist in the mixed phase regions of thunderstorms, both at the time of first lightning occurrence (Antonescu et al., 2013; Dye et al., 1989; Liu et al., 2012; Williams et al., 1989), and during active lightning production (Dye et al., 1989; Krehbiel, 1986; Lhermitte & Williams, 1985). This circumstance suggested initially that the MRL-5 radar calibration may be off, with the radar reading low in reflectivity. Other considerations, however, suggest that the modest reflectivity values in the six vertical profiles in Figure 13 are mostly valid and that other explanations may be at play. The documented TGE cases in this study do not represent the initial electrification of the day, nor do the cases with lightning (Table 4) represent the first lightning flash of the day. Quite the contrary, all of the TGEs examined are preceded by at least 30 min of electrified cloud over Aragats, with surface electric field substantially greater than fair-weather levels (or order 100 V/m). Assuming that the ice-based non-inductive charging mechanism is operating at Aragats, this observation supports the idea that pre-glaciated conditions were present for long periods prior to the TGE. In such conditions, the large surface fields characterizing the TGEs may not require the large radar reflectivity values characteristic of the initial lightning stage and the active lightning stage documented in earlier studies. Indeed, a more modest reflectivity development may be more conducive



**Table 4**

Summary of “Terminating Flashes” for Case Study Thunderstorm Ground Enhancements (All Five Terminating Flashes Noted Here are Also Shown in Figure 12)

Date (TGE time)	Terminating flash time (UT)	Lightning type for terminating flash	Flux decrease?	E field mean at peak	Description of E field during TGE
“Positive” TGEs					
4 May 2018 (0940 UT)	09:41:22	-IC (inverted dipole)	YES (Figure 12a)	30	2.85 cycle/min 1 flash/min
4 May 2018 (1005 UT)	NO	N.A. absent	N.A.	34	1.7 cycle/min 1 flash/min
30 May 2018 (0126 UT)	01:25:54	-CG (main dipole)	YES (Figure 12b)	22	1 cycle/min
“Negative” TGEs					
11 June 2016 (1148 UT)	11:45:21	+IC (main dipole)	YES (Figure 12c)	−30	4.25 flash/min
6 May 2017 (1242 UT)	12:42:24	-CG (main dipole)	YES (Figure 12d)	−31	1.5 cycle/min 0.5 flash/min
1 June 2017 (0423 UT)	NO	N.A. absent	N.A.	−32	2.7 cycle/min
Collapsing Storm Cases (Positive TGEs)					
5 Oct 2015 (0406 UT)	NO	N.A. absent	N.A.	22	4 cycle/min
8 June 2018 (1114 UT)	11:14:06	-IC (inverted dipole)	YES (Figure 12e)	19	1.5 cycle/min 0.6 flash/min

to the attainment of the larger electric field at the surface because the dielectric strength of the storm interior is compromised by the presence of large hydrometeors and turbulence. In this context, it is worth reminding that the TGEs in this study were not found by appeal to radar data to find the most lightning-active and highly reflective regions over Aragats. Instead, the maxima in surface electric field and gamma ray flux were used to guide the examination of simultaneous radar reflectivity. In the collapsing storm cases of Section 3.4, the TGEs were found at a storming stage of decidedly reduced reflectivity development and lightning activity. The present study is new in focusing on a previously unexplored phase of storm electrification characterized by the largest surface electric field but reduced vigor in both lightning activity and radar reflectivity.

This radar evidence in Figure 13 is consistent with the well-established temperature-dependent tripole structure (Bruning et al., 2007; Li et al., 2020; Simpson & Robinson, 1940; Simpson & Scrase, 1937; Takahashi et al., 1999, 2012; Zheng et al., 2018), with a graupel-driven inverted dipole at a warmer temperature, and a graupel-driven main dipole in the colder part of the troposphere. The additional documentation of collapsing storms is also consistent information in showing evidence for dominance of the main negative charge in earlier, deeper convective development, followed by dominance of the lower inverted dipole as the graupel from aloft vacates the main dipole and descends to occupy the temperature range (0°C to −10°C) linked with the inverted dipole and the LPCC. The observations of enhanced reflectivity linked with the strong  $D^6$  dependence of radar return on graupel diameter are giving information on where the temperature-dependent graupel charge resides in the respective storms.

The dominance of temperature-dependent inverted dipole structure in storms with shallow vertical development, and in widely diverse geographical locations, can be found in Bruning et al. (2007) (Oklahoma, USA), Takahashi et al. (2019); Zheng et al. (2018) (Japan), Takahashi et al. (1999) (Micronesia), Li et al. (2020) (Tibetan Plateau, China), and Svechnikova et al. (2021); Armenia). The examination of reflectivity structure directly over regions characterized by electron runaway and enhanced flux of gamma radiation in the present study serves to focus attention on the storm generator that is productive to the most intense electric field (of either polarity). This strategy is notably different from related remote sensing methods for lightning charge and for divergent outflow (microbursts) that are insensitive to the LPCC.

Wada et al. (2021) have also demonstrated a key role for graupel particles in a radar study of TGEs in winter storms in Japan. The temperature-dependent charge structures bring the storm electron accelerator closer to the

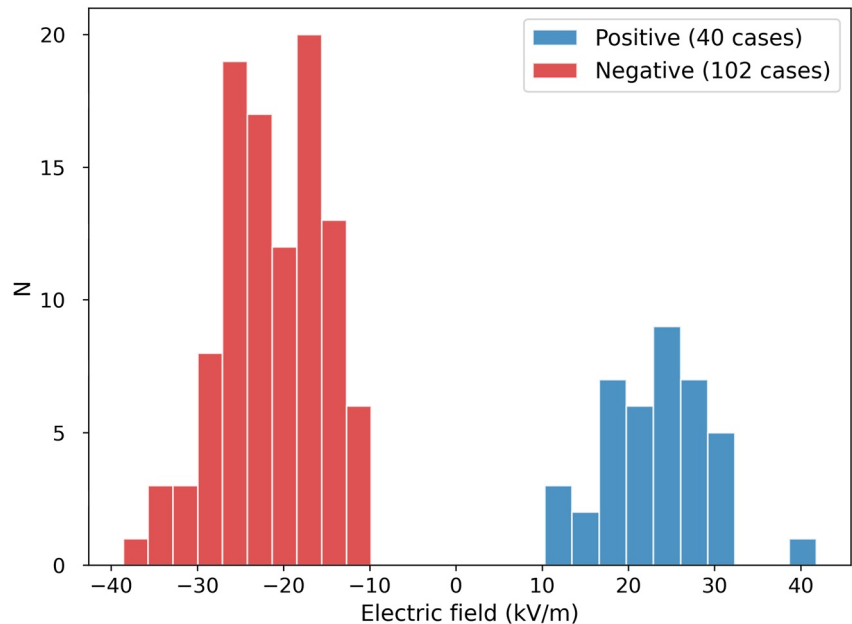


**Figure 14.** Comparative distribution of peak E field strength for Thunderstorm Ground Enhancements of both polarities for the 6-year time period 2015 to 2020.

surface in winter time. The local conditions with the warm sea of Japan under cold air promote instability and vertical air motion suitable for the formation of graupel. Torii et al. (2011) showed earlier evidence for shallow storms in Japan in winter producing enhanced gamma emission. Lacking electric field records, Wada et al. were unable to classify their TGE events as “positive” or “negative” but given the information on in situ temperature in their reflectivity cross sections, one could make some polarity categorization of TGE cases in Japan based on the radar findings from Armenia in Figure 13.

#### 4.2. Relative Prevalence of “Positive” and “Negative” TGEs

Evidence that TGEs can occur in strong electric fields of either polarity is widely known (Alexeenko et al., 2002; Chilingarian et al., 2017, 2020; Chum et al., 2020) and the phenomenon of interest here has now been documented in many countries worldwide: in Armenia (Chilingarian et al., 2010, 2011, 2012, 2017, 2021), in the Czech Republic (Kudela et al., 2017), in Italy (Aglietta, 1999; Brunetti et al., 2000), in Israel (Reuveni et al., 2017), in Japan (Torii et al., 2009, 2011; Tsuchiya et al., 2009; Wada et al., 2021), in Russia (Alexeenko et al., 2002; Gurevich et al., 2011), in Slovakia (Chum et al., 2020), in Tibet (Tsuchiya et al., 2012) and in the US (Parks, 1981; McCarthy & Parks, 1985; Eack et al., 2020; Kelley et al., 2015). This abundance of modern-day observations has renewed interest in the earlier negative results of B.F.J. Schonland and C.T.R. Wilson (Suszcynsky et al., 1996) in their initial search for this phenomenon (Schonland, 1930; Schonland & Viljoen, 1933). Given the established exceptional abundance of documented TGE events on Mt Aragats (Chilingarian, Hovsepyan, Svechnikova, & Zazyan, 2021), it is useful to quantify their relative abundance by polarity. Figure 14 shows a histogram of TGEs with well-defined polarity context for the time period 2015 to 2020 (Chilingarian et al., 2019). Maximum (minimum) electric field strengths have been extracted during positive (negative) TGEs during the full duration of half maximum (FDHM) in gamma ray flux. Negative events are more prevalent than positive events by a factor of about 2.5 to 1. Superficially speaking, this finding is consistent with the well-known summary by Benjamin Franklin (1752): “The clouds of a thunder gust are most commonly in a negative state of electricity, but sometimes in a positive state.” In this same context, it should be noted that Figure 14 is at odds with the universal prevalence of a Wilson positive dipole (Schonland, 1927; Wilson, 1916, 1920), which would cause a more pronounced polarity asymmetry, and serves as further evidence for the general tripole structure.

A second finding in Figure 14 is that no statistically significant difference is evident in the field magnitude for “positive” and “negative” TGE events. Given the speculation that the domain of breakeven electric field might

be carried down in the lower dipole of the tripole during the FEAWP (see next section), there was an expectation for a larger surface field for the “positive” TGEs. The observations in Figure 14 do not support that expectation.

### 4.3. Lightning and Electrical Behavior During Thunderstorm Ground Enhancements

The collective information on lightning flashes and gamma ray response for all eight case study storms considered in Section 3 is summarized in Table 4. A key lightning event, present in some TGE cases but not all, is the so-called “terminating flash” that occurs during the period of enhanced electric field and gamma ray flux (e.g., Chilingarian et al., 2015). The terminating flashes in the electric field records for all cases documented in Table 4 are shown in Figure 12 on the same time scale as the gamma ray flux. It is interesting that this same terminology (“terminating flash”) has been applied in earlier studies of the FEAWP (Holden et al., 1983; Lhermitte & Williams, 1984; Marshall & Winn, 1982; Moore & Vonnegut, 1977; Stolzenburg & Marshall, 1998; Williams, 1981). Given the radar evidence in this study, Field Excursion Associated with Precipitation (FEAWPs) and TGEs are in all likelihood different physical manifestations of the same thunderstorm phenomenon. FEAWPs show the same time scale as TGEs and by definition represent buildups in positive electric field and positively charged precipitation. The characteristic short times scales of FEAWPs and TGEs are attributable to the time required by graupel particles to descend through dipole extents of a few km, that is, 3,000 m at 10 m/s = 300 s = 5 min (Good examples of FEAWPs, before FEAWPs were named, can be found in the records of individual storms in the seminal studies of Simpson and Scrase (1937) and Simpson and Robinson (1940)).

The characterization of the lightning types (i.e., Intracloud (IC) and cloud-to-ground (CG)) for terminating flashes in Table 4 was made with the multiple field mill sites available around Mt. Aragats, in the same manner as in Chilingarian et al. (2017, 2020). Though the sample set in Table 4 is small, the findings are generally consistent with those of Chilingarian et al. (2017) for “negative” TGEs and with those of Chilingarian et al. (2020) for “positive” TGEs. That is to say that the “terminating flash” is an IC flash that discharges the respective dipole deemed mainly responsible for the downward electron acceleration. In two other cases (one positive TGE on 30 May 2018 and one negative TGE on 6 May 2017, a negative CG occurs that diminishes the dominant main negative charge of the electron accelerator. No cases of +CGs have been found in either the previous or present studies.

The abrupt diminishment of gamma ray flux (in the one-second-sampled flux observations and noted in Table 4) at the times of these terminating flashes is further evidence of a diminishment in dipole electric field that is causal to the enhanced flux.

Table 4 also shows that the terminating flashes are not always present in TGEs. In a study by Chilingarian et al. (2017, 2020), only events with terminating flashes were selected for analysis. As noted in Section 3.1, the case study events selected here were chosen on the basis of the DC electric field and gamma ray flux data alone. Examples of this absence of terminating flashes in the present study are shown in all three categories in Table 4. These observations may be taken as evidence that lightning is not a fundamental player in the formation of the TGE (consistent with Wilson's [1925] seminal idea), but instead is just a manifestation of the increased electric field that also drives the electron runaway.

An additional TGE diagnostic here pertains to the behavior of the electric field when the magnitude of the field is near maximum. The strong field is unsteady on time scales of tens of seconds and is occasionally reduced slightly by abrupt lightning-like field changes typically an order of magnitude smaller than that of typical terminating flashes and occurring at rates of the order of one per minute. This information is included in the right-hand column of Table 4 and discussed in more detail below.

The TGE surface field is decidedly unsteady, with variations on time scales of many tens of seconds. The variations are characterized as a rough period per cycle of variation in Table 4. It would appear that when the electric field aloft is near the breakeven value (Dwyer & Uman, 2013), there may be adjustments in cloud conductivity underway of the kind considered by Kelley et al. (2015) that prevent full-scale breakdown of lightning. Following ideas in Marshall et al. (1995), the breakeven field may be limiting the formation of full-fledged breakdown by the creation of these conductivity anomalies in the avalanche region when breakeven is achieved.

Regarding the abrupt field changes during the TGE, estimates can be made of the vertical charge moment changes  $\Delta M$  assuming they are occurring in the breakeven region above. For a dipolar charge rearrangement above a conductive ground, the abrupt change in electric field  $\Delta E$  is related to the charge moment change  $\Delta M$  by

$$\Delta M = 2\pi\epsilon D^3 \Delta E \quad (\text{coul} - \text{m})$$

where  $D$  is the distance between the dipole change and the field mill and  $\epsilon$  is the permittivity of the atmosphere. Assuming the breakeven avalanche region is directly overhead, the distance  $D$  cannot much exceed 2 km. For a field change of 1 kV/m, typical of the observations in events considered in the right-hand column of Table 4, the estimated moment change  $\Delta M$  is 440 C-m = 0.44 C-km. This value is one to two orders of magnitude smaller than typical charge rearrangements in intracloud lightning flashes (e.g., Koshak & Krider, 1989), substantiating the notion that these events do not represent storm dipole-scale breakdown (like the terminating flash) but instead involve smaller scales of the kind expected in avalanche-related conductivity anomalies (Kelley et al., 2015).

In this same context, an alternative idea in the literature envisages that a TGE may evolve into a large-scale lightning flash (Wada et al., 2019).

#### 4.4. Surface Detectability of Energetic Electrons in TGEs

On account of the recognized production of gamma rays by bremsstrahlung by stopped runaway electrons (Dwyer & Uman, 2013; Kelley et al., 2015), and by virtue of their decidedly greater range in air than energetic electrons (3.5 m for 1 MeV; 43 m for 10 MeV; Evans, 1955), gamma rays are the dominant contributor to all records of count rate on surface detectors presented in this study. The important question remains about the detectability of energetic electrons at the surface from the expected runaway/avalanche process beneath the main negative charge region.

A key consideration in addressing this question is the so-called free passage distance from the lower boundary of the breakeven region to the detectors on the surface (Chilingarian et al., 2012). To enable avalanche electrons with MeV energies to reach surface detectors, this distance needs to be small—of the order of 100 m or less. Estimates of this quantity vary widely. In the nuclear physics literature on TGEs, the free passage distance is often associated with the cloud base height (Chilingarian et al., 2012; Chilingarian, 2018a, 2018b; Chilingarian, Hovsepyan, Svechnikova, & Zazyan, 2021) which for the Aragats station (3.2 km MSL) is often 100m or less. The evidence for layers of reduced electric field due to corona space charge (Standler & Winn, 1979) would seem to require a free passage distance of at least 100 m. In contrast with these smaller estimates, the information from balloon soundings of the electric field in mountain thunderstorms in New Mexico, for example, at an observation altitude matched with that at Mt Aragats (3200 m MSL) does not show evidence for high field boundaries (or accompanying space charge anomalies) at cloud base height. Instead, the soundings show regions of an intense field which are vertically compact (typically 1, 000 m thick; Marshall et al., 2005) well above the cloud base, and relatively distant from the surface (~1 km or greater; Stolzenberg & Marshall, 2009).

Toward deciding which estimates of free passage distance are most relevant at Aragats, one can consider typical TGE behavior. In examining a large number of Aragats events, Chilingarian, Karapetyan, et al. (2013) found that typical gamma ray counts showed 3% increases during TGEs. No events were tabulated with increases less than 1% and so this value can be taken as a noise floor. In exceptional TGEs with count rate increases larger by an order of magnitude and more, and with detectable energetic electrons in more recent studies (Chilingarian, Hovsepyan, Svechnikova, & Zazyan 2021; Chilingarian, Hovsepyan, & Zazyan 2021), the energetic electron counts at the ground are of the order of 10% of the gamma ray counts. On this basis, it may be inferred that the variation in the energetic electron population will be approximately 10% of 3%, or 0.3%. This increase is below the noise floor for detection by a factor of three. On this basis, it can be concluded that the great majority of Aragats TGEs do not produce detectable energetic electrons. A reasonable explanation for this finding is that the free passage distance is large (i.e., significantly greater than 100 m).

Calculations with GEANT code (Agostinelli et al., 2003), of the kind considered earlier by Chilingarian et al. (2012) and in which the physical origins (avalanche primaries, Compton electrons, pair production, photoelectric effect) of all energetic electrons at every height can be specified, demonstrate that Compton electrons are dominant for free passage distances greater than 100–150 m. The primary electrons are largely attenuated at these

distances. All things considered, it seems likely that when energetic electrons are detected in TGEs at Aragats, an appreciable portion of them are Compton electrons, enabled by the greater range of bremsstrahlung gamma rays in the air than electrons. Further work is needed to verify the imposition of breakeven electric fields at distances of order 100 m and less from the surface when avalanche/runaway electrons might be present.

#### 4.5. Retrospective on Thunderstorms With Inverted Polarity

Special storm-scale experiments were carried out at Langmuir Laboratory in New Mexico during the summer of 1984 with the objective to invert the main dipole polarity of thunderstorms (Moore et al., 1986). A negative space charge was released from a 2-km electrified cable spanning Sawmill Canyon, as a test of the convective theory for storm electrification (Vonnegut, 1963). The evidence put forth for the inverted polarity of the storms was the appearance of a strong electric field of positive polarity on the ground beneath the storm—exactly the manifestation of “positive” TGEs in the present study. Such manifestations were documented in Figure 1 of Moore et al. (1986) on two separate days (August 2 and 15, 1984).

No accompanying radar observations were presented by Moore et al. (1986), but fortunately, time-height analyses of maximum reflectivity of the kind shown in Figures 10 and 11 have appeared in publications many years later for both storm days with “abnormal polarity”. The reflectivity plot for 2 August 1984 is found in Figure 1 of Stolzenburg and Marshall (1998), and the corresponding plot for 15 August 1984 in Figure 2 in Marsh and Marshall (1993). Though not replicated here, consistent features of both plots are weaker-than-usual vertical development (as in Figures 4c, 5c and 6c) and a decline of reflectivity contours with time in the temperature domain of the lower inverted dipole (0 to  $-10^{\circ}\text{C}$ ; as in Figures 10 and 11). In addition, Stolzenburg and Marshall (1998) identified the period of anomalous (i.e., positive) electric field on August 2 as a Field Excursion Associated with Precipitation (FEAWP). The balloon sounding of electric field on August 15 (Marsh & Marshall, 1993) during one of the two anomalous periods shows clear evidence for tripole structure (their Figure 3c).

These radar-based connections with the present work support the view that natural variability in the cloud microphysical mechanism for the tripole structure (and its variants: Mansell et al., 2010) is responsible for the “abnormal field” in cases investigated by Moore et al. (1986). This perspective was previously expressed (Williams, 2014).

#### 4.6. New Perspectives on the Lower Positive Charge Center (LPCC) in Thunderstorms

The search for TGEs at Mt Aragats with a large dataset of surface detectors and all overseen by S-band radar has placed a new spotlight on the lower positive charge center in thunderstorms. The methodology described in Section 3.1 began with a search for strong electric fields with positive polarity (i.e., dominant positive charge overhead). Figure 14 shows that nearly 30% of all documented TGEs exhibit maxima in strong positive fields. Invariably one finds in the radar observations low level precipitation cores over the location in question and with reflectivity maxima generally within 1 km of the surface sensors.

G.C. Simpson, the flag-bearer for the inverted (negative) dipole for thunderstorms (and in the present thinking the lower dipole of the temperature-dependent tripole structure), devoted attention over a period of four decades (Simpson, 1909, 1949; Simpson & Scrase, 1937; Simpson & Robinson, 1940) to the measurement of the charge on thunderstorm precipitation. In the precipitation core near the ground he found a predominance of positive charge. Simpson's long-standing scientific competitor, C.T.R. Wilson, held the opposite view (and now prevailing view) on gross thunderstorm electrical structure (Wilson, 1916; Williams, 2009). But Wilson's interests were larger scale than Simpson's, and Wilson stood back from the precipitation cores to make his lightning charge analysis with a ball antenna (Wilson, 1916, 1920). Wilson's plotted estimates of distances to his storm cores (Wilson, 1920, Figure 2) all exceeded 2 km, and so those precipitation features responsible for the TGEs in the present study were documented with radar (unavailable in Wilson's time) and shown by CAPPI plots, would have been missed. The great irony here is that the portion of the thunderstorm most important for the production of the runaway electrons in TGEs that Wilson anticipated theoretically (Wilson, 1925) and by experiment (Schonland, 1930) was excluded from his own electric field observations of thunderstorms (Wilson, 1920).

In his summary chapter on the subject of Atmospheric Electricity, physicist Richard Feynman (1964) had this to say on the lower positive charge center in thunderstorms:

“The top of the thunderstorm has a positive charge, and the bottom a negative one—except for a small local region of positive charge in the bottom of the cloud, which has caused everyone a lot of worry. No one seems to know why it is there, how important it is—whether it is a secondary effect of the positive rain coming down, or whether it is an essential part of the machinery. Things would be easier if weren't there.”

The evidence at hand on Thunderstorm Ground Enhancements supports the idea that the lower positive charge center is an essential part of the machinery, consistent with earlier assessments (Chilingarian & Mkrtchyan, 2012).

## 5. Conclusions

Vertically-resolved radar observations over a suite of sensors on Mt Aragats reaffirm the role of a temperature-dependent tripole structure as the basis for downward acceleration of electrons. The dominant central negative charge of the tripole is the repeller of the electrons for TGEs of both positive and negative polarity. “Positive” TGEs are manifest when the lower inverted dipole of the tripole is predominant in comparison with the main dipole aloft, in shallow convection. “Negative” TGEs are manifest when the main dipole is active in deeper, colder convection. The radar observations are also compatible with the ice-based precipitation mechanism in which graupel particles are the main radar targets. The physical basis for this temperature-dependent charge separation is however still poorly understood.

The temperature-dependent aspect of the storm electron accelerator increases the proximity of the main negative charge of the tripole to surface sensors at mountain stations (like Aragats), and in winter storms at sea level (as in Japan), and provides explanation for the rarity of evidence for electron runaway in low-MSL-altitude measurements beneath summer thunderstorms.

The radar-based evidence for the relatively high altitude of downward electron acceleration over Aragats make it unlikely that avalanche electrons will reach the surface detectors with free passage distances of many hundreds of meters. A more likely origin for any detected electrons at 3.2 km MSL is Compton scattering and pair production activated by longer-range bremsstrahlung gamma rays, themselves produced by runaway electron encounters with nuclei in breakeven field at higher altitude. Exceptional cases of electron-rich TGEs (Chilingarian, 2012) are deserving of further study.

The existence of TGEs in the presence of strong positive electric field brings new attention to the physical conditions of the lower positive charge center of thunderstorms. The observations reported here in the cold part of the cloud and well above the cloud base reaffirm that this feature is not the result of breaking drops (Simpson, 1949) nor corona ion capture by falling precipitation (Wilson, 1956), and that other ice-based mechanisms need to be considered.

## Data Availability Statement

All the data are available on the web page: <http://adei.crd.yerphi.am/>. Details of the subset of particle detectors used in the present study can be found in Section 2.4.

## Acknowledgments

Discussions with Brian Austin, Robert Boldi, Ken Cummins, Jim Dye, Gagik Hovsepyan, Rohan Jayaratne, Masashi Kamogawa, Thomas Marshall, Evgeny Mareev, Joan Montanya, James Rydock, David Smith, Maribeth Stolzenburg, Katya Svechnikova, Yuuki Wada and Mary Zazyan are greatly appreciated. Dr. Magomet Abshaev was particularly helpful on MRL-5 radar issues. Special thanks are due to Prof. Ashot Chilingarian for his generous access to the Aragats personnel and data archive (<http://adei.crd.yerphi.am/>) and for extensive discussions on all aspects of TGEs.

## References

- Abshaev, M., Abshaev, A., Sinkevich, A., Mikhailovskiy, Y., Popov, V., & Adzhiev, A. (2019). *Characteristics of the supercell cb thunderstorm and electrical discharges on 19 August 2015, north Caucasus: A case study*. 2019120033.
- Abshaev, M. T., Abshaev, A. M., Gekkieva, J. M., & Adzhiev, A. K. (2020). Interlink between lightning activity of hailstorms and their radar characteristics. *Journal of Physics: Conference Series*, 1604, 012010. <https://doi.org/10.1088/1742-6596/1604/1/012010>
- Aglietta, M., Alessandro, B., Antonioli, P., Arneodo, F., Bergamasco, L., Bertaina, M., et al. (1999). Gamma-rays and ionizing component during thunderstorms at Gran Sasso. *Proceedings of the 26th ICRC, Salt Lake City*, 7, 6–16. SH 3.
- Agostinelli, S., Allison, J. R., Amako, K., Apostolakis, K., Araujo, H. M., Arce, P., et al. (2003). Geant4—A simulation toolkit. *Nuclear Instruments and Methods in Physics Research Section A: Accelerators, Spectrometers, Detectors and Associated Equipment*, 506(3), 250–303.
- Alexeenko, V. V., Khaerdinov, N. S., Lidvansky, A. S., & Petkov, V. B. (2002). Transient variation of secondary cosmic rays due to atmospheric electric field and evidence for pre-lightning particle acceleration. *Physics Letter A*, 301, 299–306. [https://doi.org/10.1016/s0375-9601\(02\)00981-7](https://doi.org/10.1016/s0375-9601(02)00981-7)
- Anderson, R. V. (1966). Measurements of total current density above active snowstorms. *Journal of Atmospheric and Terrestrial Physics*, 28, 789–793. [https://doi.org/10.1016/0021-9169\(66\)90026-2](https://doi.org/10.1016/0021-9169(66)90026-2)
- Antonescu, B., Burcea, S., & Tanase, A. (2013). Forecasting the onset of cloud-to-ground lightning using radar and upper-air data in Romania. *International Journal of Climatology*, 33, 1579–1584. <https://doi.org/10.1002/joc.3533>

- Atlas, D. (1966). The balance level in convective storms. *Journal of the Atmospheric Sciences*, 23, 635–651. [https://doi.org/10.1175/1520-0469\(1966\)023<0635:tblics>2.0.co;2](https://doi.org/10.1175/1520-0469(1966)023<0635:tblics>2.0.co;2)
- Austin, B. A. (2001). *Schonland: Scientist and Soldier*: Institute of Physics Publishing.
- Avakyan, K., Arakelyan, A., Chilingarian, A., Daryan, A., Kozliner, L., Mailyan, B., et al. (2013). NaI detector network at Aragats. NaI detector network at Aragats. *Journal of Physics: Conference Series*, 409, 012223. <https://doi.org/10.1088/1742-6596/409/1/012218>
- Bateman, M. G., Marshall, T. C., Stolzenburg, M., & Rust, W. D. (1999). Precipitation charge and size measurements inside a New Mexico mountain thunderstorm. *Journal of Geophysical Research*, 104, 9643–9653. <https://doi.org/10.1029/1998jd200118>
- Battan, L. J. (1973). *Radar observations of the atmosphere* (p. 324). University of Chicago Press.
- Brunetti, S. C., Galli, M., Giovannini, G., & Pagliarini, A. (2000). Gamma ray bursts of atmospheric origin in the MeV energy range. *Geophysical Research Letters*, 27, 1599–1602. <https://doi.org/10.1029/2000gl003750>
- Bruning, E. C., Rust, W. D., Schuur, T. J., MacGorman, D. R., Krehbiel, P. R., & Rison, W. (2007). Electrical and polarimetric radar observations of a multicell storm in TEXAS. *Monthly Weather Review*, 135, 2525–2544. <https://doi.org/10.1175/mwr3421.1>
- Chilingarian, A. (2014). Thunderstorm ground enhancements—Model and relation to lightning flashes. *Journal of Atmospheric and Solar-Terrestrial Physics*, 107, 68–76. <https://doi.org/10.1016/j.jastp.2013.11.004>
- Chilingarian, A. (2018a). Long lasting low energy thunderstorm ground enhancements and possible Rn-222 daughter isotopes contamination. *Physics Review D*, 98, 022007. <https://doi.org/10.1103/physrevd.98.022007>
- Chilingarian, A. (2018b). The SEVAN worldwide network of particle detectors: 10 years of operation. *Advances in Space Research*, 50(273–1177(18)), 30172–30178.
- Chilingarian, A., Arakelyan, K., Avakyan, K., Babayan, V., Bostanjyan, V., Chilingarian, S., et al. (2005). Correlated measurements of secondary cosmic ray fluxes by the Aragats Space-Environmental Center monitors. *Nuclear Instruments & Methods in Physics Research, Section A*, 543(2–3), 483–496. <https://doi.org/10.1016/j.nima.2004.12.021>
- Chilingarian, A., Hovsepyan, G., & Hovhannisyanyan, A. (2011). Particle bursts from thunderclouds: Natural particle accelerators above our heads. *Physical Review D*, 83, 06200. <https://doi.org/10.1103/physrevd.83.062001>
- Chilingarian, A., Hovsepyan, G., Khanikyan, G., Reymers, A., & Soghomonyan, S. (2015). Lightning origination and thunderstorm ground enhancements terminated by a lightning flash. *Europhysics Letters*, 110. <https://doi.org/10.1209/0295-5075/110/49001>
- Chilingarian, A., Hovsepyan, G., Soghomonyan, S., Zazyan, M., & Zelenyy, M. (2018). Structures of the intracloud electric field supporting origin of long-lasting thunderstorm ground enhancements. *Physical Review D*, 98, 082001. <https://doi.org/10.1103/physrevd.98.082001>
- Chilingarian, A., Hovsepyan, G., Svechnikova, E., & Zazyan, M. (2021). Electrical structure of the thundercloud and operation of the electron accelerator inside it. *Astroparticle Physics*, 132, 10261. <https://doi.org/10.1016/j.astropartphys.2021.102615>
- Chilingarian, A., Hovsepyan, G., & Zazyan, M. (2021). *Measurement of TGE particle energy spectra: An insight into the cloud charge structure* (pp. 21–100038). EPL.
- Chilingarian, A., Kants, Y., Mareev, E., Pokhsaryan, D., Rakov, V. A., & Soghomonyan, S. (2017). Types of lightning discharges that abruptly terminate enhanced fluxes of energetic radiation and particles observed at ground level. *Journal of Geophysical Research: Atmospheres*, 122, 7582–7599. <https://doi.org/10.1002/2017jd026744>
- Chilingarian, A., Karapetyan, T., & Melkumyan, L. (2013). Statistical analysis of the thunderstorm ground enhancements (TGEs) detected on Mt. Aragats. *Advances in Space Research*, 52, 1178–1192. <https://doi.org/10.1016/j.asr.2013.06.004>
- Chilingarian, A., Khanikyan, Y., Rakov, V. A., & Soghomonyan, S. (2020). Termination of thunderstorm-related bursts of energetic radiation and particles by inverted intracloud and hybrid lightning discharges. *Atmospheric Research*, 223. <https://doi.org/10.1016/j.atmosres.2019.104713>
- Chilingarian, A., Mailyan, B., & Vanyan, L. (2012). Recovering of the energy spectra of electrons and gamma rays coming from thunderclouds. *Atmospheric Research*, 114–115, 1–16. <https://doi.org/10.1016/j.atmosres.2012.05.008>
- Chilingarian, A., & Mkrtchyan, H. (2012). Role of the lower positive charge region (LPCR) in initiation of the Thunderstorm Ground Enhancements (TGEs). *Physical Review D*, 86, 072003. <https://doi.org/10.1103/physrevd.86.072003>
- Chilingarian, A., Mkrtchyan, H., Karapetyan, G., Chilingarian, S., Sargsyan, B., & Arestakesyan, A. (2019). Catalog of 2017 thunderstorm ground enhancement (TGE) events observed on Aragats. *Scientific Reports*, 9. Article number: 6253. <https://doi.org/10.1038/s41598-019-42786-7>
- Chilingarian, A., Vanyan, L., & Mailyan, B. (2013). Observation of thunderstorm ground enhancements with intense fluxes of high-energy electrons. *Astroparticle Physics*, 48, 1–7. <https://doi.org/10.1016/j.astropartphys.2013.06.006>
- Chilingarian, S., Beglarian, A., Kopmann, A., & Voekling, S. (2010). Advanced data extraction infrastructure: Web based system for management of time series data. *Journal of Physics: Conference Series*, 219, 042034. <https://doi.org/10.1088/1742-6596/219/4/042034>
- Chum, J., Langer, R., Base, T., Kollarik, M., Strharsky, I., Diendorfer, G., & Rusz, J. (2020). Significant enhancements of secondary cosmic rays and electric field at the high mountain peak of Lomnický štít in High Tatras during thunderstorms. *Earth Planets and Space*, 72, 28. <https://doi.org/10.1186/s40623-020-01155-9>
- Dwyer, J. R., & Uman, M. A. (2013). The physics of lightning. *Physics Reports*, 534(4), 147–241.
- Dye, J. E., Winn, W. P., Jones, J. J., & Breed, D. W. (1989). The electrification of New Mexico thunderstorms I. Relationship between precipitation development and the onset of electrification. *Journal of Geophysical Research*, 94, 8643–8656. <https://doi.org/10.1029/jd094i06p08643>
- Eack, K. B., Suszcynsky, D. M., Beasley, W. H., Roussel-Dupre, R., & Symbalisty, E. M. D. (2020). Gamma-ray emissions observed in a thunderstorm anvil. *Geophysical Research Letters*, 27, 185–188. <https://doi.org/10.1029/1999GL010849>
- Evans, R. D. (1955). *The Atomic Nucleus*: McGraw-Hill.
- Feynman, R. P., Leighton, R. B., & Sands, M. (1964). *The Feynman Lectures on Physics*. (Vol. II). Addison-Wesley. Chapter 9.
- Franklin, B. (1752). *Philosophical Transactions of the Royal Society*, 47, 289.
- Gurevich, A. V., Chubenko, A. P., Karashtin, A. N., Antonova, V. P., Mitko, G. G., Naumov, A. S., et al. (2011). The effective growth of gamma-ray background during a thunderstorm. *Physics Letter A*, 375, 4003–4006. <https://doi.org/10.1016/j.physleta.2011.09.038>
- Holden, D. N., Holmes, C. R., Moore, C. B., Winn, W. P., Cobb, J. W., Griswold, J. E., & Lytle, D. M. (1983). Local charge concentrations in thunderclouds. In L. H. Ruhnke & J. Latham (Eds.), *Sixth International Conference on Atmospheric Electricity, Proceedings in Atmospheric Electricity* (pp. 179–183). Deepak.
- Jacobson, E. A., & Krider, E. P. (1976). Electrostatic field changes produced by Florida lightning. *Journal of the Atmospheric Sciences*, 33, 103–117. [https://doi.org/10.1175/1520-0469\(1976\)033<0103:efcpbf>2.0.co;2](https://doi.org/10.1175/1520-0469(1976)033<0103:efcpbf>2.0.co;2)
- Jayarathne, R., & Saunders, C. P. R. (1984). The “raingush”: Lightning and the lower positive charge center. *Journal of Geophysical Research*, 89, 11816–11818. <https://doi.org/10.1029/jd089i07p11816>
- Karakhanian, A., Jrbashyan, R., Trifonov, V., Philip, H., Arakelian, S., Avagyan, A., et al. (2003). Volcanic hazards in the region of the Armenian nuclear power plant. *Journal of Volcanology and Geothermal Research*, 126, 31–62. [https://doi.org/10.1016/s0377-0273\(03\)00115-x](https://doi.org/10.1016/s0377-0273(03)00115-x)
- Karunarathna, N., Marshall, T. C., Karunarathne, S., & Stolzenburg, M. (2017). Initiation locations of lightning flashes relative to radar reflectivity in four small Florida thunderstorms. *Journal of Geophysical Research: Atmospheres*, 122, 6565–6591. <https://doi.org/10.1002/2017jd026566>

- Kelley, N. A., Smith, D. M., Dwyer, J. R., Splitt, M., Lazarus, S., Martinez-McKinney, F., et al. (2015). Relativistic electron avalanches as a thunderstorm discharge competing with lightning. *Nature Communications*. <https://doi.org/10.1038/ncomms8845>
- Koloskov, B., Zimin, B., Beliaev, V., Seregin, Y., Chernikov, A., Petrov, V., et al. (1996). Results of experiments on convective precipitation enhancement in the Camaguey Experimental Area. *Journal of Applied Meteorology*, 35, 1524–1534. [https://doi.org/10.1175/1520-0450\(1996\)035<1524:roeocp>2.0.co;2](https://doi.org/10.1175/1520-0450(1996)035<1524:roeocp>2.0.co;2)
- Koshak, W. J., & Krider, E. P. (1989). Analysis of lightning field changes during active Florida thunderstorms. *Journal of Geophysical Research*, 94, 1165–1186. <https://doi.org/10.1029/jd094id01p01165>
- Krehbiel, P. R. (1981). An analysis of the electric field change produced by lightning, Vol. I and II, Report No. T-11, *New Mexico Mining and Technology*, Socorro.
- Krehbiel, P. R. (1986). The electrical structure of thunderstorms. In *The Earth's Electrical Environment* (pp. 90–113). National Acad. Press.
- Krehbiel, P. R., Brook, M., Lhermitte, R. L., & Lennon, C. L. (1983). Lightning charge structure in thunderstorms, Proc. In L. H. Ruhnke & J. Latham (Eds.), *Atmospheric Electricity*. Deepak Publishing.
- Kudela, K., Chum, J., Kolbrik, M., Langer, R., Strharsky, I., & Base, J. (2017). Correlations between secondary cosmic ray rates and strong electric fields at Lomnický štít. *Journal of Geophysical Research: Atmospheres*, 122, 10700–10710. <https://doi.org/10.1002/2016jd026439>
- Kuettner, J. (1950). The electrical and meteorological conditions inside thunderclouds. *Journal of Meteorology*, 7, 322–332. [https://doi.org/10.1175/1520-0469\(1950\)007<0322:teamci>2.0.co;2](https://doi.org/10.1175/1520-0469(1950)007<0322:teamci>2.0.co;2)
- Lhermitte, R., & Williams, E. (1984). Doppler radar and electrical activity observations of a mountain thunderstorm. *22nd Conference on Radar Meteorology*, American Meteorological Society.
- Lhermitte, R. M., & Williams, E. R. (1985). Thunderstorm electrification: A case study. *Journal of Geophysical Research*, 90, 6071–6078. <https://doi.org/10.1029/jd090id04p06071>
- Li, Y., Zhang, G., & Zhang, Y. (2020). Evolution of the charge structure and lightning discharge characteristics of a Qinghai-Tibet Plateau thunderstorm dominated by negative cloud-to-ground flashes. *Journal of Geophysical Research: Atmospheres*, 125, e2019JD031129. <https://doi.org/10.1029/2019JD031129>
- Liu, C., Cecil, D. J., Zipser, E. J., Kronfeld, K., & Robertson, R. (2012). Relationships between lightning flash rates and radar reflectivity vertical structures in thunderstorms over the tropics and subtropics. *Journal of Geophysical Research*, 117, D06212. <https://doi.org/10.1029/2011JD017123>
- Maier, L. M., & Krider, E. P. (1986). The charges that are deposited by cloud-to-ground lightning in Florida. *Journal of Geophysical Research*, 91, 13275–13289. <https://doi.org/10.1029/jd091id12p13275>
- Mansell, E. R., Ziegler, C. L., & Bruning, E. C. (2010). Simulated electrification of a small thunderstorm with two-moment bulk microphysics. *Journal of the Atmospheric Sciences*, 67, 171–194. <https://doi.org/10.1175/2009jas2965.1>
- Markson, R., & Anderson, B. (1988). *Negative Polarity Charge in Cloud Tops*, 8th International Conf. on Atmospheric Electricity, 438–446, June 13–18.
- Marsh, S. J., & Marshall, T. C. (1993). Charged precipitation measurements before the first lightning flash in a thunderstorm. *Journal of Geophysical Research*, 98, 16605–16611. <https://doi.org/10.1029/93jd00419>
- Marshall, T. C., McCarthy, M. P., & Rust, W. D. (1995). Electric field magnitudes and lightning initiation in thunderstorms. *Journal of Geophysical Research*, 100, 7097–7103. <https://doi.org/10.1029/95jd00020>
- Marshall, T. C., & Stolzenburg, M. (1998). Estimates of charge densities in thunderstorms. *Journal of Geophysical Research*, 103, 19769–19775. <https://doi.org/10.1029/98jd01674>
- Marshall, T. C., Stolzenburg, M., Maggio, C. R., Coleman, L. M., Krehbiel, P. R., Hamlin, T., et al. (2005). Observed electric fields associated with lightning initiation. *Geophysical Research Letters*, 32, L03813. <https://doi.org/10.1029/2004GL021802>
- Marshall, T. C., & Winn, W. P. (1982). Measurements of charged precipitation in a New Mexico thunderstorm: Lower positive charge centers. *Journal of Geophysical Research*, 87, 7141–7157. <https://doi.org/10.1029/jc087ic09p07141>
- McCarthy, M., & Parks, G. K. (1985). Further observations of X-rays inside thunderstorms. *Geophysical Research Letters*, 12, 393–396. <https://doi.org/10.1029/GL012i006p00393>
- Moore, C. B. (1965). Charge generation in thunderstorms. In S. C. Coronti (Ed.), *Problems in atmospheric electricity* (pp. 255–262). Elsevier.
- Moore, C. B., & Vonnegut, B. (1977). The thundercloud. In R. H. Golde (Ed.), *Lightning* (Vol. I, pp. 51–98). Academic Press.
- Moore, C. B., Vonnegut, B., Rolan, T. D., Cobb, J. W., Holden, D. N., Hignight, R. T., et al. (1986). Abnormal polarity of thunderclouds grown from negatively charged air. *Science*, 233, 1413–1416. <https://doi.org/10.1126/science.233.4771.1413>
- Moskowitz, S., Ciach, G. J., & Krajewski, W. F. (1994). Statistical detection of anomalous propagation in radar reflectivity patterns. *Journal of Atmospheric and Oceanic Techniques*, 11, 1026–1034.
- Parks, G. K., Mauk, B. H., Spiger, R., & Chin, J. (1981). X-ray enhancements detected during thunderstorm and lightning activities. *Geophysical Research Letters*, 8, 1176–1179. <https://doi.org/10.1029/gl008i011p01176>
- Pena, A. O. R., Perez, M., Naranjo, R., Fernandez, L., Barreiras, A., Martinez, A., & Rodriguez, M. D. (2000). Modernization of the Cuban weather radar network. *Physics and Chemistry of the Earth*, 25, 1169–1171. [https://doi.org/10.1016/s1464-1909\(00\)00173-8](https://doi.org/10.1016/s1464-1909(00)00173-8)
- Raymond, D. J., Solomon, R., & Blyth, A. M. (1991). Mass fluxes in New Mexico Mountain thunderstorms from radar and aircraft measurements. *Quarterly Journal of Royal Meteorological Society*, 117, 587–621. <https://doi.org/10.1002/qj.49711749909>
- Reuveni, Y., Yair, Y., Price, C., & Steinitze, G. (2017). Ground level gamma-ray and electric field enhancements during disturbed weather: Combined signatures from convective clouds, lightning and rain. *Atmospheric Research*, 196, 142–150. <https://doi.org/10.1016/j.atmosres.2017.06.012>
- Schonland, B. F. J. (1927). The polarity of thunderclouds. *Proceedings of the Royal Society A*, 118, 233–251.
- Schonland, B. F. J. (1930). Thunder-storms and the penetrating radiation. *Proceedings of the Royal Society A*, 130, 37–63.
- Schonland, B. F. J., & Viljoen, J. P. T. (1933). On a penetrating radiation from thunderclouds. *Proceedings of the Royal London. Series A, Containing Papers of a Mathematical and Physical Character*, 140(No. 841), 314–333.
- Simpson, G. C. (1909). On the electricity of rain and its origin in thunderstorms. *Philosophical Transactions*, A209, 379–413.
- Simpson, G. C. (1949). Atmospheric electricity during the last 50 years, Part I: The normal electrical field in the atmosphere. *Weather*, 4, 104–108. <https://doi.org/10.1002/j.1477-8696.1949.tb01019.x>
- Simpson, G. C., & Robinson, G. D. (1940). The distribution of electricity in thunderclouds, II. *Proceedings of the Royal Society A*, 177, 281–329.
- Simpson, G. C., & Scrase, F. J. (1937). The distribution of electricity in thunderclouds. *Proceedings of the Royal Society A*, 114, 376–401.
- Standler, R. B., & Winn, W. P. (1979). Effects of coronae on electric fields beneath thunderstorms. *Quarterly Journal of Royal Meteorological Society*, 105, 285–302. <https://doi.org/10.1002/qj.49710544319>
- Stolzenburg, M., & Marshall, T. C. (1998). Charged precipitation and electric field in two thunderstorms. *Journal of Geophysical Research*, 103, 19777–19790. <https://doi.org/10.1029/98jd01675>



- Stolzenberg, M., & Marshall, T. C. (2009). Electric field and charge structure in lightning-producing clouds. In H.-D. Betz, U. Schumann, & P. Laroche (Eds.), *Chapter 3 in lightning: Principles, Instruments and Applications: Review of modern lightning research* (pp. 57–82). Springer.
- Stolzenberg, M., Marshall, T. C., & Krehbiel, P. R. (2015). Initial electrification to the first lightning flash in New Mexico thunderstorms. *Journal of Geophysical Research: Atmospheres*, *120*, 11253–11276. <https://doi.org/10.1002/2015jd023988>
- Suszczynsky, D. M., Roussel-Dupre, R., & Shaw, G. (1996). Ground-based search for X-rays generated by thunderstorms and lightning. *Journal of Geophysical Research*, *101*, 23505–23516. <https://doi.org/10.1029/96JD02134>
- Svechnikova, E. K., Ilin, N. V., Mareev, E. A., & Chilingarian, A. A. (2021). Characteristic features of the clouds producing thunderstorm ground enhancements. *Journal of Geophysical Research: Atmospheres*, *126*, e2019JD030895. <https://doi.org/10.1029/2019jd030895>
- Takahashi, T. (1978). Riming electrification as a charge generation mechanism in thunderstorms. *Journal of the Atmospheric Sciences*, *35*, 1536–1548. [https://doi.org/10.1175/1520-0469\(1978\)035<1536:reaacg>2.0.co;2](https://doi.org/10.1175/1520-0469(1978)035<1536:reaacg>2.0.co;2)
- Takahashi, T. (2012). Precipitation charge distributions and evolution of East Asian rainbands. *Atmospheric Research*, *118*, 304–323. <https://doi.org/10.1016/j.atmosres.2012.07.016>
- Takahashi, T., Sugimoto, S., Kawano, T., & Suzuki, K. (2019). Microphysical structure and lightning initiation in Hokuriku winter clouds. *Journal of Geophysical Research: Atmospheres*, *124*(23), 13156–13158. <https://doi.org/10.1029/2018jd030227>
- Takahashi, T., Tajiri, T., & Sonoi, Y. (1999). Charges on graupel and snow crystals and the electrical structure winter thunderstorms. *Journal of the Atmospheric Sciences*, *56*, 1561–1578. [https://doi.org/10.1175/1520-0469\(1999\)056<1561:cogasc>2.0.co;2](https://doi.org/10.1175/1520-0469(1999)056<1561:cogasc>2.0.co;2)
- Torii, T., Sugita, T., Kamogawa, M., Watanbe, Y., & Kusunoki, K. (2011). Migrating source of energetic radiation generated by thunderstorm activity. *Geophysical Research Letters*, *38*, L24801. <https://doi.org/10.1029/2011gl049731>
- Torii, T., Sugita, T., Tanabe, S., Kimura, Y., Kamogawa, M., Yajima, K., et al. (2009). Gradual increase of energetic radiation associated with thunderstorm activity at the top of Mt. Fuji. *Geophysical Research Letters*, *36*, L13804. <https://doi.org/10.1029/2008gl037105>
- Tsuchiya, H., Enoto, T., Torii, T., Nakazawa, K., Yuasa, T., Torii, S., et al. (2009). Observation of an energetic radiation burst from mountaintop thunderclouds. *Physics Research Letters*, *102*, 255003. <https://doi.org/10.1103/physrevlett.102.255003>
- Tsuchiya, H., Hibino, K., Kawata, K., Hotta, N., Tateyama, N., Ohnishi, M., et al. (2012). Observation of thundercloud-related gamma rays and neutrons in Tibet. *Physical Review D: Particles and Fields*, *85*, 092006. <https://doi.org/10.1103/physrevd.85.092006>
- Visser, P. J. M. (2001). The Storm-Structure-Severity method for the identification of convective storm characteristics with conventional weather radar. *Meteorological Applications*, *8*, 1–10. <https://doi.org/10.1017/s1350482701001013>
- Vonnegut, B. (1963). Some facts and speculations concerning the origin and role of thunderstorm electricity, Severe Local Storms. *Meteorological Monograph, No.*, *5*, 224–241. [https://doi.org/10.1007/978-1-940033-56-3\\_11](https://doi.org/10.1007/978-1-940033-56-3_11)
- Wada, Y., Enoto, T., Kubo, M., Nakazawa, K., Shinoda, T., Yonetoku, D., et al. (2021). Meteorological aspects of gamma-ray glows in winter thunderstorms. *Geophysical Research Letters*, *48*(7), e2020GL091910. <https://doi.org/10.1029/2020gl091910>
- Wada, Y., Enoto, T., Nakamura, Y., Furuta, Y., Yuasa, T., Nakazawa, K., et al. (2019). Gamma ray glows preceding downward terrestrial gamma-ray flash. *Communications on Physics*, *2*, 67.
- Williams, E., Weber, M., & Orville, R. (1989). The relationship between lightning type and convective state of thunderclouds. *Journal of Geophysical Research*, *94*, 13213–13220. <https://doi.org/10.1029/jd094id11p13213>
- Williams, E. R. (1981). *Thunderstorm electrification: Precipitation vs convection*, Ph.D. Dissertation. Department of Earth, Atmospheric and Planetary Sciences, MIT.
- Williams, E. R. (1989). The triple structure of thunderstorms. *Journal of Geophysical Research*, *94*, 13151–13167. <https://doi.org/10.1029/jd094id11p13151>
- Williams, E. R. (1990). *Lightning and Microbursts in Convective Clouds, 16th Conference on Severe Local Storms* (Vol. 738–743). American Meteorological Society, Kananaskis Provincial.
- Williams, E. R. (2006). Problems in lightning physics—The role of polarity asymmetry. *Plasma Sources Science and Technology*, *15*, S91–S108.
- Williams, E. R. (2009). C.T.R Wilson versus G.C Simpson: Fifty years of controversy in atmospheric electricity. *Atmospheric Research*, *91*(2–4), 259–271.
- Williams, E. R. (2014). Charge structure and geographical variation of thunderclouds. In V. Cooray (Ed.), *The Lightning Flash* (2nd ed.). The Institution of Engineering and Technology.
- Wilson, C. T. R. (1916). On some determinations of the sign and magnitude of electric discharges in lightning flashes. *Proceedings of the Royal Society, A*, *92*, 555–574.
- Wilson, C. T. R. (1920). Investigations on lightning discharges and on the electric field of thunderstorms. *Philosophical Transactions A*, *221*, 73–115.
- Wilson, C. T. R. (1923). Investigation on X-rays and  $\beta$ -rays by the cloud method. Part II.  $\beta$ -rays. *Proceedings of the Royal Society London, Series A*, *104*, 192–212.
- Wilson, C. T. R. (1925). The acceleration of  $\beta$ -particles in strong electric fields such as those of thunderclouds. *Proceedings of the Cambridge Philosophical Society*, *22*, 534–538.
- Wilson, C. T. R. (1929). Some thundercloud problems. *Journal of the Franklin Institute*, *208*, 1–12.
- Wilson, C. T. R. (1956). A theory of thundercloud electricity. *Proceedings of the Royal Society A*, *236*, 297–317.
- Zheng, D., Wang, D., Zhang, Y., Wu, T., & Takagi, N. (2018). Charge regions indicated by LMA flashes in Hokuriku's winter thunderstorms. *Journal of Geophysical Research: Atmospheres*, *124*(13), 7179–7206. <https://doi.org/10.1029/2018JD030060>